The Cryosphere Discuss., 9, 1077–1131, 2015
www.the-cryosphere-discuss.net/9/1077/2015/
doi:10.5194/tcd-9-1077-2015

The Cryosphere Discussions
Open Access

Arctic sea ice area in CMIP3 and CMIP5 climate model ensembles – variability and change

V. A. Semenov[1,2,3], **T. Martin**[1], **L. K. Behrens**[1,*], **and M. Latif**[1,4]

[1]GEOMAR Helmholtz Centre for Ocean Research, Kiel, Germany
[2]A. M. Obukhov Institut of Atmospheric Physics Russian Academy of Sciences, Moscow, Russia
[3]Institute of Geography Russian Academy of Sciences, Moscow, Russia
[4]Kiel University, Kiel, Germany
[*]now at: University of Bremen, Bremen, Germany

Received: 22 January 2015 – Accepted: 2 February 2015 – Published: 20 February 2015

Correspondence to: T. Martin (tmartin@geomar.de)

Published by Copernicus Publications on behalf of the European Geosciences Union.

Abstract

The shrinking Arctic sea ice cover observed during the last decades is probably the clearest manifestation of ongoing climate change. While climate models in general reproduce the sea ice retreat in the Arctic during the 20th century and simulate further sea ice area loss during the 21st century in response to anthropogenic forcing, the models suffer from large biases and the model results exhibit considerable spread. The last generation of climate models from World Climate Research Programme Coupled Model Intercomparison Project Phase 5 (CMIP5), when compared to the previous CMIP3 model ensemble and considering the whole Arctic, were found to be more consistent with the observed changes in sea ice extent during the recent decades. Some CMIP5 models project strongly accelerated (non-linear) sea ice loss during the first half of the 21st century.

Here, complementary to previous studies, we compare results from CMIP3 and CMIP5 with respect to regional Arctic sea ice change. We focus on September and March sea ice. Sea ice area (SIA) variability, sea ice concentration (SIC) variability, and characteristics of the SIA seasonal cycle and interannual variability have been analysed for the whole Arctic, termed Entire Arctic, Central Arctic and Barents Sea. Further, the sensitivity of SIA changes to changes in Northern Hemisphere (NH) averaged temperature is investigated and several important dynamical links between SIA and natural climate variability involving the Atlantic Meridional Overturning Circulation (AMOC), North Atlantic Oscillation (NAO) and sea level pressure gradient (SLPG) in the western Barents Sea opening serving as an index of oceanic inflow to the Barents Sea are studied.

The CMIP3 and CMIP5 models not only simulate a coherent decline of the Arctic SIA but also depict consistent changes in the SIA seasonal cycle and in the aforementioned dynamical links. The spatial patterns of SIC variability improve in the CMIP5 ensemble, particularly in summer. Both CMIP ensembles depict a significant link between the SIA and NH temperature changes. Our analysis suggests that, on average, the sensitivity

TCD
9, 1077–1131, 2015

of SIA to external forcing is enhanced in the CMIP5 models. The Arctic SIA variability response to anthropogenic forcing is different in CMIP3 and CMIP5. While the CMIP3 models simulate increased variability in March and September, the CMIP5 ensemble shows the opposite tendency. A noticeable improvement in the simulation of summer SIA by the CMIP5 models is often accompanied by worse results for winter SIA characteristics. The relation between SIA and mean AMOC changes is opposite in September and March, with March SIA changes being positively correlated with AMOC slowing. Finally, both CMIP ensembles demonstrate an ability to capture, at least qualitatively, important dynamical links of SIA to decadal variability of the AMOC, NAO and SLPG. SIA in the Barents Sea is strongly overestimated by the majority of the CMIP3 and CMIP5 models, and projected SIA changes are characterized by a large spread giving rise to high uncertainty.

1 Introduction

The Northern High Latitudes exhibit the most visible signs of the climate change during the last decades. The surface warming in the Arctic has been at least twice as strong as the global average warming during recent decades (e.g., IPCC AR5, 2013). This Arctic amplification and its mechanism is under intense debate, with variations of sea ice, atmospheric and oceanic heat transport and radiative forcing feedbacks all having been suggested as possible mechanisms (Holland and Bitz, 2003; Alexeev et al., 2005; Graversen et al., 2008; Serreze et al., 2009; Screen and Simmonds, 2010; Walsh, 2014). The Arctic warming has been accompanied by a rapid summer sea ice extent (SIE) decline of the order of about 10 % per decade since 1979 (the start of satellite observations) that has considerably, by a factor of two, accelerated in the 21st century (Stroeve et al., 2007, 2012). This is probably the most apparent, accurately observed and influential manifestation of regional climate change on the Earth. The complicated mechanisms involved in the Arctic sea ice loss and its dramatic consequences make it "a grand challenge of climate science" (Kattsov et al., 2010). On the contrary, Antarctic

TCD
9, 1077–1131, 2015

SIE depicted a slight increase during the satellite era (Cavalieri and Parkinson, 2012), further demonstrating the complex physics operating in sea ice variability and change.

Reconstructions suggest that current summer Arctic sea ice retreat is likely to be unprecedented in the last millennium (Kinrad et al., 2011; Halfar et al., 2014), although a clear manifestation of strong multidecadal variability is indicated by observations and models (Polyakov et al., 2003; Divine and Dick, 2006; Semenov, 2008; Semenov and Latif, 2012; Day et al., 2012; Miles et al., 2014). For example, regional scale records, in particular in the eastern Arctic, also indicate considerable summer sea ice area reduction during the Early Twentieth Century Warming (ETCW) (Polyakov et al., 2003; Alekseev et al., 2007, 2009). The winter sea ice cover reduction during the satellite era is considerably smaller than that in summer and there are indications that it may be comparable to that during the ETCW (Semenov and Latif, 2012). The winter sea ice retreat, however, has a great potential to impact the large-scale atmospheric circulation by modulating the intense turbulent heat fluxes from the ocean surface to the atmosphere, which may force anomalous and extreme weather regimes (see Vihma, 2014, for a review). Recently, a link between summer weather extremes and sea ice retreat has also been suggested (Screen, 2013; Tang et al., 2013; Guo et al., 2013).

Arctic sea ice thickness has also experienced a dramatic decrease, by roughly a half, during the last three decades, as suggested by different observation methods (Vaughan et al., 2013). We note that the uncertainty of these estimates is much higher than that for the sea ice area (Johannessen et al., 2004; Schweiger et al., 2011).

The analyses of long-term historical sea ice cover variations in the Entire Arctic are restricted to the second half of the 20th century and early 21st century, for which sufficiently reliable gridded sea ice concentration data based on regular instrumental observations are available (Walsh and Johnson, 1979). Since 1979, passive microwave satellite data provide the most accurate estimates of the sea ice extent with high spatial and temporal resolution that, however, are dependent on the data retrieval algorithm (Kattsov et al., 2010; Ivanova et al., 2014).

TCD
9, 1077–1131, 2015

Global climate models reproduce the Arctic sea ice area/extent decline during the recent observational period (from the mid-20th until beginning of the 21st century) when forced by estimates of historical anthropogenic and natural forcings. Simulations with climate models participating in the World Climate Research Programme (WCRP) Coupled Model Intercomparison Project Phase 3 (CMIP3) (Meehl et al., 2007) used in the Fourth Assessment Report of the IPCC (IPCC: Climate Change, 2007) in general noticeably underestimate the observed September sea ice extent reduction. Based on CMIP3 models, only about 47 to 57 % of the sea ice extent decrease over the satellite era can be attributed to anthropogenic forcing, leaving the rest either for natural variability, model or forcing errors (Stroeve et al., 2007). Several models, which compare well to observations, predicted a seasonally ice free Arctic already before 2040 (Wang and Overland, 2009), with the ensemble mean reaching this level around 2080 (Alekseev et al., 2009). However, the model results depict a very large spread (Stroeve et al., 2007; Alekseev et al., 2009). The important role of increasing greenhouse gas concentrations has also been suggested by solely empirical data analyses (Johannessen, 2004; Notz and Marotzke, 2012) that, however, presumably exclude the possibility of strong internal multidecadal fluctuations (Bengtsson et al., 2004; Wood et al., 2010).

Arctic sea ice may be strongly influenced by atmospheric and oceanic internal variability, including North Atlantic Oscillation (NAO), Atlantic Multidecadal Osillation (AMO) and Barents Sea inflow (BSI) variability (Dickson et al., 2000; Bengtsson et al., 2004; Semenov, 2008; Day et al., 2012; Smedsrud et al., 2013; Miles et al., 2014). The links between natural forcing factors and Arctic sea ice, however, may be essentially non-stationary and non-linear (Semenov, 2008; Semenov et al., 2009; Smedsrud et al., 2013). Again, a relatively short observational record hinders a detailed analysis of the variability mechanisms, while climate models suffer from large biases, particularly on a regional scale.

A new generation of climate models included in the CMIP5 (Taylor et al., 2012) ensemble employed in IPCC AR5 (IPCC AR5, 2013) have demonstrated in general a better agreement with the observed September Arctic SIE trends, thus implying a larger

TCD
9, 1077–1131, 2015

(52–67 %) contribution of the anthropogenic forcing (Stroeve et al., 2012). The CMIP5 models project a seasonally ice free Arctic sooner than the CMIP3 models (Stroeve et al., 2012; Wang and Overland, 2009). Model spread and uncertainty of the 21st century projections in CMIP5, however, remained similar to those in CMIP3 (Stroeve et al., 2012). We note that the above assessments relate to September trends of the sea ice extent for the whole Arctic, termed Entire Arctic.

To better understand mechanisms underlying Arctic sea ice cover variations and to estimate uncertainties of projected future changes, the results of simulations with different model ensembles should be inter-compared and validated against observations. One has to keep in mind that updated observations provide a reference line for climate models to match by tuning parameters within the range of uncertainty (Mauritsen et al., 2012). This is particularly the case with the Arctic sea ice area that exhibited about twice as strong decline during the early 21st century than during previous decades, thus having provided different perspectives for CMIP3 and CMIP5 modelers. Total Arctic sea ice area (and volume) is sensitive to parameters' choice in climate models, in particular poorly constrained ice albedo, and therefore can be easily tuned (Eisenman et al., 2007; Hodson et al., 2013). The reliability of model results can be better assessed by analyzing regional changes of sea ice and also investigating changes in its seasonal cycle, variability and links to atmospheric and oceanic dynamics in different generations of climate models. Here, we follow this strategy.

Further, most analyses of the CMIP3 and CMIP5 models have so far been performed for either of the ensembles and focused on the changes of sea ice cover in the Entire Arctic in September and (less so) in March (e.g., Stroeve et al., 2007, 2012; Alekseev et al., 2009; Kattsov et al., 2010; Massonnete et al., 2012). Here, we also present analyses of simulated sea ice area (SIA) variability in March and September and its sensitivity to global warming on a regional scale. Furthermore, the seasonal cycle amplitude is also investigated. A major focus of this study is on the intercomparison of the CMIP3 and CMIP5 model ensembles.

TCD
9, 1077–1131, 2015

Past climate variations and projected changes in the Arctic differ considerably between individual regions (Overland et al., 1997; Venegas and Mysak, 2000; Semenov and Bengtsson, 2003; Rogers et al., 2013). Some regions may be of particular importance for Arctic climate variability, for example the Barents Sea. Strong variability of oceanic inflow, intense heat losses from the sea surface and positive feedbacks in the regional coupled atmosphere–sea ice–ocean system lead to enhanced variability in this region that affects the climate of the Entire Arctic (Bengtsson et al., 2004; Semenov and Bengtsson, 2003; Semenov, 2008; Semenov et al., 2009; Smedsrud et al., 2013). The sea ice conditions in the Barents Sea itself are impacted by the North Atlantic Oscillation (NAO) (Kwok, 2000), the leading mode of internal atmospheric variability in the Northern Extratropics during winter (van Loon and Rogers, 1978) and by the Atlantic Multidecadal Oscillation (Semenov, 2008; Miles et al., 2014), the leading large-scale pattern of multidecadal variability in North Atlantic surface temperature. Additionally, the oceanic inflow into the Barents Sea is affected by the NAO (Dickson et al., 2000), and the link between all these processes may be non-stationary, as suggested by climate models and observations (Goosse and Holland, 2005; Semenov, 2008; Smedsrud et al., 2013). Petoukhov and Semenov (2010) showed that reduced sea ice concentrations in the Barents-Kara Sea region may exert a strong effect on the European climate through changes in atmospheric circulation, leading to anomalously cold winters over Eurasia. Furthermore, the Barents Sea is the region where climate models exhibit the strongest sea ice error and bias in simulating present day temperatures. This is also the region where climate models project the strongest warming by the end of the 21st century (Flato et al., 2013; IPCC, 2013). Thus, the Barents Sea is one key region on which we focus in our analyses. The Central Arctic is another region chosen for analysis. Until recent decades, and in preindustrial control integrations with climate models, this region has been covered by thick multi-year sea ice nearly all year round. Thus, in contrast to the Barents Sea, SIA variations there have been small and past SIA evolution in this region may be well suited to assess the models' ability to realistically simulate sea ice variability and change.

TCD
9, 1077–1131, 2015

The CMIP models differ considerably not only in simulated sea ice changes, but also in their representation of the temperature response to external forcing. Whether the differences in the simulated sea ice changes are related to the different warming pace or whether they represent regional and sea ice model-related uncertainties remains an open question. Therefore, we assess the sensitivity of sea ice changes in the Arctic region to Northern Hemisphere warming in both CMIP model ensembles. We also study the amplitude of the SIA seasonal cycle. It characterizes the sharpness of the seasonal contrasts and is an important parameter influencing various climate impacts, be they physical, chemical, biological or economical. For example, a shortened sea ice season may lead to considerable advantages for marine transportation using Northern Sea Route and North-West Passage (Khon et al., 2010). Furthermore, changes in sea ice area and thickness in the Arctic basin are accompanied by changes in variability (Holland et al., 2008). It still remains unclear how the interannual sea ice variability may change in a warmer climate. Therefore the interannual variability in the CMIP3 and CMIP5 models is analysed as well. As was outlined above, internal climate variability modes including NAO and AMO were found (basing on empirical data analysis and some model simulations) to affect Arctic sea ice variations. Simulating such links is a challenge for climate models as it requires the simulation of dynamical processes in the atmosphere and ocean, as well as their interaction with sea ice dynamics. Here, we assess CMIP models' ability to reproduce these links (in terms of linear relations) and estimate how these links may change in a warmer climate.

The paper is organized as follows. In the next section, we provide a description of the data sets and methodology used in this study. In section three, the results are presented. They include changes in spatial sea ice concentration (SIC) variability, analysis of September and March SIA for the Entire Arctic, Barents Sea and Central Arctic regions, sensitivity of SIA changes to Northern Hemispheric warming, changes in SIA variability, SIA seasonal cycle amplitude evolution, links to NAO, AMO and BSI indices. The main conclusions and a discussion of the results can be found in section four.

TCD
9, 1077–1131, 2015

2 Data and methods

The analysis is based on the World Climate Research Programme's (WCRP's) Coupled Model Intercomparison Projects phase 3 (CMIP3) and phase 5 (CMIP5) multimodel dataset covering the period 1900–2100 (see Tables 1 and 2). Observations are presented from the gridded HadISST1 data (Rayner et al., 2003) providing sea surface temperature (SST) and sea ice concentration (SIC) since 1870. The observational data prior to 1953 are sparse and highly inhomogeneous (Walsh and Chapman, 2001). The recent study by Semenov and Latif (2012) suggested that there must have been a strong negative sea ice extent anomaly (comparable to the current decrease) in winter during the ETCW that is not present in the HadISST1 dataset. Therefore, we analyzed HadISST1 data only starting from 1950.

From the CMIP database, 20C3M (CMIP3) and historical (CMIP5) runs for the 20th century incorporating observed climate forcings complemented by climate change simulations using A1B-scenario (CMIP3) and representative concentration pathway (RCP) future scenarios RCP 4.5 and RCP 8.5 (CMIP5) for the 21st century were analysed. Only one (the first) member of each climate model ensemble is used, since models have different numbers of ensemble simulations, some of them just one. Observational and all model data were interpolated onto a $2^{\circ} \times 2^{\circ}$ grid for intercomparison.

Sea ice area (SIA, area-integrated sea ice concentration) is analysed here. The results thus are quantitatively different to those studies using sea ice extent (SIC) for analysis. When using sea ice extent (SIE), a grid cell area that is covered by more than 15 % ice is fully integrated to the total value, whereas SIA accounts only for the cell fraction covered by sea ice. This leads to larger SIE values compared to analyses based on SIA and may even result in qualitative differences in climatic trends (Cavalieri and Parkinson, 2012). Sea ice area is calculated as integrated sea ice concentration multiplied by grid box area. In the following, we present results for the Entire Arctic, Central Arctic and Barents Sea. One should keep in mind that model differences can also result from different horizontal resolutions and land–sea masks. For example, smaller islands

TCD
9, 1077–1131, 2015

like Svalbard are not resolved in some models. Models with a coarse coastline resolution are marked with an asterisk in Table 1. The Central Arctic is defined as the basin north of 80° N. The Barents Sea is defined here as the area between 70 and 80° N and 20° E (Svalbard) and 62° E (Novaya Zemlya) (see Gloersen et al., 1992).

The analyses mostly use September and March values, corresponding on average to the minimum and maximum of the annual sea ice extent evolution, respectively. Seasonal averages are used in sensitivity analyses. The amplitude and phase of the seasonal cycle are calculated based on monthly values with the Fourier approach of Granger and Hatanaka (1964). The time series have been detrended by subtracting fourth order polynomial trends prior to the calculation of the annual harmonic of the monthly mean sea ice data.

3 Results

3.1 Spatial SIC variability

3.1.1 Spatial structure of interannual SIC variability in 1950–2000

The interannual variability of the Arctic sea ice concentration (SIC) is characterized by a distinct spatial structure. Figure 1 shows the observed and multi-model mean interannual variability of SIC in March and September during the second half of the 20th century, represented by SDs (Standard deviation) calculated from the monthly data (after subtracting long-term climatic trend). The observations (Fig. 1a and b) show that the regions with high interannual variability basically follow the average sea ice margin. Highest variability regions in winter (March) are located in the Atlantic sector in the Barents, Greenland and Labrador Seas, regions characterized by strong wintertime atmospheric and oceanic variability, and in the Pacific sector in the Bering Sea and Sea of Okhotsk, another region of strong atmospheric variability. In summer (September), the areas of high interannual variability are more symmetrically distributed, encompass-

TCD
9, 1077–1131, 2015

ing internal Arctic Seas and centred on the thickest sea ice region close to Canadian Archipelago.

The model SIC data are presented as multi-models means, i. a. by averaging the interannual variability over all ensemble members (models included here are according to Tables 1 and 2). Both ensembles qualitatively capture the main features of the observed variability structure. The models on average distinctly underestimate (by about 50 % in the regions of highest observed variability) the variability both in March and September. The simulated variability in March is also marked by an obvious westward shift of the highest variability area in the Barents Sea, indicating an overestimation of sea ice area in the Sea by a large number of models (Fig. 1c). Extensive sea ice coverage is also reflected in September by a southward extension of the variability area (Fig. 1d). The major difference between CMIP5 and CMIP3 is related to an apparent improvement in the simulated variability. In March, the simulated variability by CMIP5 models (Fig. 1e) agrees much better with observations compared to former CMIP results. In particular, the region of strong variability in the Barents Sea is much better simulated than in CMIP3. However, the spatial spread of the sea ice edge is still too large in all regions.

In summer (September), the variability in CMIP5 models is strongly enhanced in the internal Arctic Seas (Fig. 1f) in comparison to the CMIP3 ensemble and better fits to the observations. Much better simulation of the interannual variability along the ice margins, however, is accompanied by overestimated variability in large parts of the central Arctic region, suggesting an overall increase of summer SIC sensitivity to heat balance variations at the atmosphere–ocean interface. To sum up this part, the CMIP5 ensemble on average simulates higher interannual variability than CMIP3 models that is in most regions in a better agreement with the observations, particularly in the Atlantic sector. A clear improvement in reproducing September SIC interannual variability in CMIP5 can be reported.

TCD
9, 1077–1131, 2015

3.1.2 Simulated interannual SIC variability in 2050–2100

The CMIP models, when forced by scenarios of future anthropogenic forcing, simulate a considerable change in the interannual SIC variability pattern in the second half of the 21st century in comparison to 1950–2000 (Fig. 1c–f). Figures 2 and 3 show changes in SIC variability for the 2050–2100 period simulated by the CMIP3 models under scenario SRES A1B and CMIP5 models using the RCP 4.5 and RCP 8.5 scenarios for March and September respectively. It should be noted that RCP 8.5 corresponds to the strongest radiative forcing, whereas RCP 4.5 is weaker than the forcing of SRES A1B used in CMIP3. The latter, in terms of the CO_2 concentrations at the end of the 21st century, is between the two RCPs (e.g., Meinshausen et al., 2011). A direct comparison of the results from the two CMIP ensembles is therefore not possible. Further, since sea ice dynamics is highly nonlinear, a simple linear interpolation may lead to erroneous interpretations.

The CMIP models project for the 21st century marked changes in the interannual variability during winter (March) in response to anthropogenic forcing (Fig. 2). The left panels of Fig. 2 depict the patterns of interannual SIC variability during 2050–2100 in CMIP ensembles, the right panels the changes relative to 1950–2000. In March, the SIC variability is strongly increased close to ice margins and towards the inner Arctic (Fig. 2). This is consistent with higher sensitivity of thinner ice to variations of atmospheric and oceanic heat fluxes. The strongest increase in the SIC variability during March is projected in the RCP 8.5 scenario exhibiting the largest radiative forcing, with a noticeable increase even in the Central Arctic, indicating much less compact sea ice in winter in this region (Fig. 2f). Interestingly, the CMIP5 models under the RCP 4.5 scenario, which is weaker than SRES A1B, show a stronger variability increase in some regions in comparison to the CMIP3 models. This again suggests a higher sensitivity of SIC in the CMIP5 ensemble. Reduced variability outside the sea ice margin reflects the complete removal of sea ice in those areas in the projected future. The same reasoning explains September SIC variability changes (Fig. 3). Complete disappearance

TCD
9, 1077–1131, 2015

of the sea ice cover in the marginal Arctic Seas leads to zero variability and results in a decrease in comparison to 1950–2000; multi-year sea ice in the Central Arctic becomes thinner and more variable. The smaller area of increased SIC variability in the Central Arctic in CMIP5 RCP 8.5 results from the stronger sea ice retreat in response to the stronger forcing.

3.2 Changes in Arctic sea ice area

Changes in sea ice area (SIA) for the Entire Arctic, Central Arctic and Barents Sea as simulated and projected by the CMIP3 and CMIP5 models and as observed are depicted in Figs. 4 and 5 for March and September, respectively. We show only the RCP 8.5 scenario from CMIP5.

3.2.1 Entire Arctic

In March (Fig. 4a and b), the CMIP5 ensemble-mean bias for SIA during the observation period becomes larger than in CMIP3, reaching almost 2.0×10^6 km^2 as compared to 1.5×10^6 km^2 in CMIP3. The ensemble-mean SIA decrease by the end of the 21st century amounts to 3.0×10^6 km^2 in CMIP3 (SRES A1B) and 5.5×10^6 km^2 in CMIP5 (RCP 8.5). The CMIP5 ensemble-mean SIA of is about 10×10^6 km^2 by the end of the 21st century, which is still comparable to the observed present day conditions of about 13×10^6 km^2. Two models (NCAR-CCSM3.0 and GISS-MODEL-E-R) show a very sharp decrease to less than 4×10^6 km^2, while three others (MPI-ECHAM5, INM-CM3, and UKMO-HadGEM1) simulate excessive SIA exceeding 20×10^6 km^2 during the 20th century (Fig. 4b). Due to such "outliers", the overall model spread becomes larger in CMIP5 compared to CMIP3.

In contrast to our findings for the SIA in March, a clear improvement of September SIA is seen in the CMIP5 models during 1950–2100 (Fig. 5a). When considering the Entire Arctic, the multi-model mean September SIA decreases by 4×10^6 km^2 by the end of 21st century in CMIP3 (Fig. 5a) and by 5×10^6 km^2 in CMIP5 (Fig. 5b). Practically

TCD
9, 1077–1131, 2015

all CMIP5 models (except for GFDL-CM2.0) simulate an ice-free Arctic by the end of the 21st century under the very strong RCP 8.5 scenario. Sea ice extent projections from the CMIP5 RCP 4.5 ensemble has been analysed by Stroeve et al. (2012) and these featured a decrease that, despite the weaker forcing, was comparable to that calculated from the CMIP3 SRES A1B ensemble. Several CMIP5 models (Fig. 5b) project a strongly accelerating decrease of SIA around the 2030s, indicating a potential instability or "tipping point" (Lenton et al., 2008). The very recent observed accelerated Arctic sea ice loss is, however, still not fully captured in the multi-model mean, which may suggest a significant contribution from internal variability (Day et al., 2012) or that the models are too conservative. The latter could imply that Arctic sea ice will continue retreating at the accelerated rate observed during the early 21st century and an ice-free Arctic by 2020 (Alekseev et al., 2009; Wang and Overland, 2009). The former is suggested by the strong decadal variability simulated in a number of climate models (Semenov and Latif, 2012) with amplitude large enough to explain the recent accelerated sea ice retreat. To sum up this part, the CMIP5 models better reproduce the long-term trend of the Entire Arctic SIA in September for the observational period (when predominantly historical radiative forcing was applied).

We note that our results for the Entire Arctic differ somewhat from those reported by Stroeve et al. (2007, 2012). The reason is related to using different sea ice cover variables and differences in methodology. Stroeve et al. (2007, 2012) use sea ice extent that sums up grid cells with more than 15 % area covered by sea ice. This makes the total results dependent on grid cell area and the contribution of grid cells with low sea ice concentration. Further, Stroeve et al. (2012) restrict the analysis to a subset of models excluding "outliers", while we consider the whole ensembles.

3.2.2 Central Arctic

In winter, the Central Arctic is totally covered by sea ice in all models (Fig. 4c, d) until around the 2050s, when SIA begins to shrink. The ensemble-mean decrease by the end of the 21st century is rather modest, amounting to 0.15×10^6 km^2 and $0.45 \times$

TCD
9, 1077–1131, 2015

10^6 km^2 in CMIP3 and CMIP5, respectively. Again, the same CMIP5-low "outliers" as for the Entire Arctic exhibit an outstanding drop down to 0.5×10^6 km^2. In September, the ensemble mean is smaller than the observed SIA. This indicates that the majority of models underestimate the September SIA in the Central Arctic during the observation period in both CMIP3 and CMIP5 (Fig. 5c and d), with CMIP5 being slightly worse. When forced by the RCP 8.5 scenario, a majority of the CMIP5 models show very steep SIA reduction within 2–3 decades, from the present day level to complete sea ice removal. The large inter-model spread in the two ensembles results from different timing of fast SIA decline, with a distinct group of CMIP5 models clustering around 2030 (Fig. 5d).

3.2.3 Barents Sea

As it is already outlined in the Introduction, the Barents Sea region may play a key role for large-scale atmospheric variability, atmosphere–ocean feedbacks and even multi-decadal climate variations in the Arctic and Northern Hemisphere (Semenov and Bengtsson, 2003; Bengtsson et al., 2004; Semenov et al., 2009, 2010; Smedsrud et al., 2013). With SIA on average constituting only about 5 % of the total Arctic SIA, the Barents Sea makes a minor contribution when considering the total Arctic SIA mean, trends and variability. Uncertainties in simulations of the sea ice cover in the Barents Sea thus contribute a minor part to the total sea ice bias, but may lead to a significant difference in simulating the extra-tropical atmospheric circulation in winter (e.g., Petoukhov and Semenov, 2010; Yang and Christinsen, 2012; Inoue et al., 2012), as well as in the atmosphere–ocean feedbacks which are important for decadal to multi-decadal variability in the Arctic sector (Mysak and Venegas, 1998; Bengtsson et al., 2004; Goosse and Holland, 2005).

In March, the mean SIA for the observation period is fairly similar in both model data sets, strongly overestimating the observed value. CMIP5 models on average simulate a stronger SIA reduction, thus better fitting observations (Fig. 4e and f). It is worth men-

TCD
9, 1077–1131, 2015

tioning that mean model bias is stronger than the observed trend during 1950–2010. Both in September and March, the simulated SIA in individual runs exhibits strong decadal variability that may in part explain the observed decadal variations, in particular the sharp SIA decrease in 2005. The models (both CMIP3 and CMIP5) on average strongly overestimate SIA in the Barents Sea in September (by a factor of 3 to 4) and exhibit a very large spread from a nearly ice free Barents Sea in the 20th century to almost fully ice covered conditions (Fig. 5e and f). The Barents Sea is currently almost ice free in summer, while the models on average simulate such conditions by the end of the 21st century or around 2050 in the CMIP3 and CMIP5 ensembles, respectively. CMIP5 models reproduce September SIA noticeably better.

3.3 Sensitivity of sea ice area to surface air temperature changes

The large SIA spread in the model results is related to various reasons. Highly intense atmospheric variability in high latitudes, complicated ocean dynamics, model uncertainties related to ice albedo parameter choice and simulation of Arctic cloud cover are among the factors leading to divergent estimates (Eisenman et al., 2007; Karlsson and Svensson, 2013; Koenigk et al., 2014). One of the most important questions in this respect is how future SIA change is related to global warming rate. This issue was addressed in several studies for total summer Arctic sea ice in the CMIP3 models, with the aim of reducing uncertainty in model projections with respect to reaching ice free Arctic conditions (Zhang, 2010; Winton, 2011; Mahlstein and Knutti, 2011; Massonnet et al., 2012).

We calculated the sea ice area sensitivity to changes in Northern Hemisphere (NH) surface air temperature (SAT) as the ratio between SIA and SAT changes averaged over the periods 1970–2000 and 2070–2100 based on the CMIP models' data. The scatter diagrams in Fig. 6 (winter) and Fig. 7 (summer) show the sensitivities obtained from CMIP3 (SRES A1B scenario) and CMIP5 (RCP 8.5) for the Entire Arctic, Central Arctic and Barents Sea. The intra-ensemble regressions and correlations are summarized in Table 3 (which also includes results from CMIP5-RCP 4.5). For the Entire

TCD
9, 1077–1131, 2015

Arctic SIA, a robust linear dependence of winter sea ice area on the NH SAT change can be seen (see Fig. 6a and b) with a correlation coefficient close to −0.8 in both ensembles. The slope of the regression line in CMIP3-A1B is -1.92×10^6 km^2 °C^{-1}, -1.58×10^6 km^2 °C^{-1} in CMIP5-RCP8.5 and -1.31×10^6 km^2 °C^{-1} in CMIP5-RCP4.5. Thus, winter SIA in the CMIP5 models is less sensitive to NH SAT increase in comparison to the CMIP3 models. Further, the different sensitivities in CMIP5-RCP 4.5 and CMIP5-RCP8.5 suggest that a stronger forcing leads to accelerated summer SIA decrease (Fig. 7a and b). These differences are, however, within the model uncertainty range (Table 3). We note that the models depicting very strong NH warming by the end of the 21st century (about 6 °C and even more) exhibit SIA sensitivities which strongly depart from the regression line, suggesting non-linear effects.

Central Arctic SIA does not exhibit a robust relationship to NH SAT in winter in the CMIP models (Fig. 6c and d, Table 3). This is due to the modest SIA changes in many models, even by the end of the 21st century. The stronger regression slope in the CMIP5 models is related to the aforementioned outliers, whereas the majority of models do not show significant changes even under RCP 8.5 scenario. Barents Sea winter SIA change as a function of NH SAT (Fig. 6e and f) is characterized by a large intra-model spread which is particularly strong for the CMIP5 ensemble. This implies higher uncertainty in the future projections, which is important in the context of the strong and non-linear impact of Barents SIA on the atmospheric circulation over the northern continents (Petoukhov and Semenov, 2010; Yang and Christensen, 2012).

Summer sensitivities (Fig. 7) exhibit noticeable differences in comparison to those obtained for winter. Whereas the CMIP3 ensemble depicts a rather close link between NH SAT and SIC changes (Fig. 7a), CMIP5 models show a weaker dependence on surface air temperature changes (Fig. 7b). This is partly related to the stronger radiative forcing which drives ice free conditions by the end of the century in the majority of the models. Thus, the presented sensitivities largely depend on the SIA values during 1970–2000 that are almost randomly distributed. Therefore, the intermediate forcing scenario RCP 4.5 leads to a stronger sensitivity (Table 3). This is also valid for the

TCD
9, 1077–1131, 2015

Central Arctic SIA (Fig. 7c and d). However, for the Barents Sea (Fig. 7e and f), neither of the CMIP ensembles shows a statistically significant correlation of intra-model SIA differences and NH SAT changes. This, as well, may be explained by the disappearance of sea ice already by the middle of the 21st century, making SIA sensitivity strongly dependent on the present-day state.

3.4 Changes in SIA seasonal cycle amplitude

The stronger decrease of the sea ice area (SIA) during September in comparison with March, as observed and simulated by the CMIP models (Figs. 4 and 5), implies an increase in the seasonal cycle amplitude (Fig. 8). This can be clearly seen in the observations for the Entire Arctic and Central Arctic (Fig. 8a–d). The CMIP models tend to underestimate the observed trend. At the end of the 20th century, the amplitude of the SIA seasonal cycle for the Entire Arctic is about 5.9×10^6 km^2 in CMIP5-RCP 8.5 (5.0×10^6 km^2 in CMIP3-A1B), which amounts to about 40 % (35 %) of the maximum winter sea ice area. The amplitude increases during the 21st century. In the CMIP5-RCP 8.5 ensemble, the amplitude reaches maximum values of 6.6×10^6 km^2 (55 % of the March sea ice area) around 2060 and then decreases to present day values. This behaviour is related to the fact that many models become seasonally ice free after 2050 and seasonal cycle amplitude change due to slower winter sea ice decrease. Amplitude increase in CMIP3-A1B models proceeds monotonically reaching about 5.5×10^6 km^2 to the end of the 21st century.

During the overlapping period, the observations show a much (at least three times) stronger trend in the seasonal cycle amplitude of the Entire Arctic SIA than both the CMIP3-A1B and CMIP5-RCP 8.5 ensemble means (Fig. 8a and b). Further, the models noticeably overestimate the observed amplitude during 1950–2010. In this respect, the CMIP5 models even exhibit a much larger bias than those from CMIP3.

The major portion of the simulated increase of the SIA seasonal cycle amplitude for the Entire Arctic is caused by changes in the Central Arctic (Fig. 8c and d). In this region, both model ensembles reasonably well reproduce the observed trend, but

TCD
9, 1077–1131, 2015

still show a strong positive bias, which is particularly visible in CMIP5-RCP 8.5. In the Barents Sea region, the observations indicate a small reduction in the SIA seasonal cycle amplitude, with strong decadal variability superimposed (Fig. 8e and f). Here, both ensembles are characterized by very large spread. The ensemble-mean trends do not correspond to the most probable trends, with a majority of models falling into the tails of the distributions. The ensemble-mean SIA seasonal cycle amplitude decrease after 2000 in CMIP5-RCP 8.5 results from the majority of the models predicting an ice free Barents Sea in summer, with 5 very strong outliers that simulate excessive ice cover after 2050 (Fig. 8f). In CMIP3-A1B, the ensemble mean does not exhibit much change during the 21st century. Strong decadal to inter-decadal variability of the sea ice cover in the Barents Sea is simulated by the majority of the models, be they from CMIP3-A1B or CMIP5-RCP 8.5, consistent with the notion that the Barents Sea is a region that is strongly affected by natural variations of the oceanic inflow and atmospheric circulation.

The evolution of the seasonal cycle phase during the 20th and 21st century is characterized by very large uncertainties (not shown). When considering the Entire Arctic, ensemble-mean phase changes from both CMIP3-A1B and CMIP5-RCP 8.5 amount to only about 5 days during the whole 21st century. The observations do not indicate a long-term trend, but strong decadal variability in all regions (not shown).

3.5 Changes in interannual variability

Climate change not only affects the annual-mean and seasonal cycle of Arctic sea ice, but also its interannual variability. Changes in interannual variability are of large societal relevance, as they may are important for sea ice prediction and the frequency of occurrence of extreme SIA anomalies. We analyze the SD of interannual SIA variability during the following three time periods: preindustrial (using the results of the preindustrial control integrations), 1950–2000 and 2050–2100. The long-term trend has been subtracted as a fourth order polynomial fit before computing SDs. Calculations for the preindustrial period and 1950–2000 are very similar. Therefore, we present only results

TCD
9, 1077–1131, 2015

for the latter period. Figure 9 shows the SD of the SIA for the Entire Arctic in the individual models for March and ratio between SD in September and March (R_{SM}) for both CMIP ensembles.

During the 20th century period (1950–2000), the interannual variability in March is considerably weaker in CMIP3 than in CMIP5 (Fig. 9a) and fits better to observations. The results shown in Fig. 9 indicate that the ratio R_{SM} is strongly linked to the strength of the interannual variability in March. Models that exhibit higher variability in March, exceeding about 3×10^5 km^2 ($R_{SM} > 1$), tend to have enhanced variability in September with a stronger enhancement to that in March. Models with variability in March that is below the threshold have reduced variability in September with an opposite dependence. In the observations, interannual variability in September is almost 2.5 times stronger than in March (Fig. 9a). During 1950–2000, the CMIP3 models on average reproduce the observed variability in March, but strongly underestimate it in September. The CMIP5 models simulate a much higher variability in March, which is almost twice as strong as that observed, but a more realistic variability in September.

Changes in interannual variability simulated during the second half of the 21st century are principally different in CMIP3 and CMIP5. In CMIP3, the number of models with $R_{SM} > 1$ markedly increases and variability in March is slightly enhanced (Fig. 9b). In contrast, the majority of the CMIP5 models project a strong reduction of interannual SIA variability in both March and September. Variability is more strongly reduced in RCP 4.5 than in RCP 8.5, rendering RCP 4.5 being very close to CMIP3 during 1950–2000 in terms of the ensemble means. The projected future increase of SIA interannual variability in September in CMIP3 is consistent with what may be expected from observational data analysis by Holland et al. (2008), Holland and Stroeve (2011) and Goosse et al. (2009). Holland et al. (2008) argued that thinner September sea ice melts faster, but can also faster converge and form big areas. Goosse et al. (2009) also suggested that the increasing interannual SIA variability in September is related to thinner sea ice. Holland and Stroeve (2011) propose less impact of the atmospheric circulation

TCD
9, 1077–1131, 2015

on the September sea ice variability because of a shift in the surface pressure (SLP) anomalies in the Eastern Arctic.

3.6 Sea ice variability and AMOC

The North Atlantic (NA) Ocean transports heat poleward, reducing imbalance of radiative fluxes between low and high latitudes (e.g.; Trenberth and Caron, 2001). The Atlantic Meridional Overturning circulation (AMOC) makes the major contribution to the oceanic heat transport in the NA with about 1 PW of heat at about 30° N (where in general the maximal heat transport is observed) (e.g., Delworth and Mann, 2000, and references therein). Observations from various sources and model simulations suggest a strong multi-decadal variability of the AMOC that impacts poleward heat transport, NA surface temperatures and turbulent heat fluxes and Arctic sea ice (Koltermann et al., 1999; Latif et al., 2004; Semenov, 2008; Polyakov et al., 2010; Day et al., 2012; Miles et al., 2014). Multi-decadal variability in the North Atlantic may noticeably contribute to globally averaged SAT variability (e.g., Semenov et al., 2010) and is a major source of uncertainty in SAT projections for the 21st century (e.g., Kravtsov and Spannagle, 2008).

3.6.1 SIA change and AMOC

The AMOC is projected to weaken with global warming due to stronger warming and enhanced fresh water input in high latitudes (e.g., Schneider et al., 2007). This implies less heat transported to the Arctic that may mitigate sea ice loss, constituting a dynamical negative feedback. Thus the relationship of the Arctic SIA to the mean AMOC may indicate which factor (AMOC weakening or temperature increase) dominates SIA change. We present here an overview of SIA sensitivity in CMIP models to changes in mean AMOC. Figure 10 shows changes of March and September SIA from 1970–2000 to 2070–2100 as a function of an AMOC index (defined as the maximum of the overturning streamfunction at 30° N) in CMIP3-A1B and CMIP5-RCP 8.5. We note that

TCD
9, 1077–1131, 2015

AMOC data are not available from all CMIP models. Both CMIP ensembles generally depict a negative correlation between March SIA and AMOC changes (Fig. 10a and c). In both ensembles, models with stronger SIA reduction depict less AMOC weakening, again with a closer link for the CMIP5-RCP 8.5 ensemble. This suggests that in winter, AMOC slowing and the associated reduction in oceanic poleward heat transport plays a more important role for SIA than in summer, with a reduced AMOC strength overriding the local effects of radiative forcing.

The relationship between the AMOC strength and September SIA change is opposite to that in March (Fig. 10b and d). In CMIP5-RCP 8.5, this relation is much (about 5 times) stronger and the model spread smaller (correlation 0.68) than in CMIP3 (correlation 0.20), which may partly be explained by the stronger forcing. Thus, models with a stronger Arctic SIA loss also simulate a stronger weakening of the AMOC, indicating that AMOC weakening does not determine the SIA response in the Entire Arctic. One may expect that both the AMOC and SIA changes within the model ensembles are negatively correlated with hemispheric SAT. This, however, is not the case. Both the CMIP3 and CMIP5 models do not show any significant link between NH SAT and AMOC strength changes (not shown).

3.6.2 SIA and multidecadal AMOC variability

In climate models, decadal to multidecadal AMOC variability strongly impacts Arctic sea ice, even determining Arctic surface climate variability on these time scales. Further, deep ocean convection sites and oceanic transports through the Fram Strait and Barents Sea Opening are affected (Jungclaus et al., 2005; Goosse and Holland, 2005; Semenov, 2008; Mahajan et al., 2012). We analyse the linear relationships between multidecadal AMOC and SIA variability during 1900–1970 and 2030–2100 (Fig. 11). Again, long-term trends represented by a fitted fourth order polynomial have been removed and correlations computed for 9 year running means. The strength of correlations during 1900–1970 and 2070–2100 are depicted on the x and y axis, respectively. Such a presentation helps to demonstrate how the correlation may change in the future.

TCD
9, 1077–1131, 2015

If the correlation-pair of a particular model is located in the bottom-left or upper-right quadrant means that the link between the multidecadal variability in the AMOC and SIA is (qualitatively) the same in the 20th and 21st centuries. Location in the two other quadrants indicates a change of the sign in the relation. Since oceanic heat transport variability associated with the AMOC is strongest during winter, we analyse only March SIA.

During 1900–1970, the majority of the CMIP3 models simulate a negative correlation between AMOC and SIA variations in the Entire Arctic and Barents Sea (Fig. 11a and c). This is consistent with previous modelling studies and the physical notion of decreased SIA associated with enhanced poleward heat transport. However, some models depict a positive correlation in the 20th or 21st centuries, or in both. The majority of the CMIP5 models also show a negative correlation between multidecadal AMOC and SIA variations in the Entire Arctic (Fig. 11b) and Barents Sea (Fig. 11d), with roughly half of models showing a change in the sign of the relationship during the 21st century. It should be noted in this context that variations in oceanic and atmospheric heat transport may be in anti-phase (referred to as "Bjerknes compensation"). This relation may also vary with time, as shown in climate model simulations (Jungclaus and Koenigk, 2010).

3.7 SIA and large scale atmospheric variability

Arctic SIA variations are also linked to large-scale atmospheric circulation changes. The major mode of atmospheric winter time variability in the Extratropics is the North Atlantic Oscillation (NAO) (van Loon and Rogers, 1978; Hurrel, 1995). Although hypotheses have been put forward that the NAO is impacted by the ongoing global warming (e.g., Kuzmina et al., 2005) and low-frequency oceanic variability such as that linked to the AMOC (Peings and Magnusdottir, 2014), the NAO spectrum may not be distinguishable from white noise with statistical confidence (Wunsch, 1999; Semenov et al., 2008). The NAO has a strong impact on SIA in the Barents Sea, a region with strongest interannual and decadal SIA variability in winter. Barents Sea SIA is to a large extent

TCD
9, 1077–1131, 2015

directly affected by the atmospheric circulation and oceanic inflow that itself is also modulated by atmospheric variability (Smedsrud et al., 2013). Therefore, the Barents Sea represents a good region to assess the models' performance with respect to the simulation of important physical links. The oceanic inflow to the Barents Sea is impacted by the NAO, although this link is essentially non-stationary (Dickson et al., 2000; Bengtsson et al., 2004; Semenov, 2008; Smedsrud et al., 2013). The inflow is primarily wind-driven and thus depends on the strength of the southwesterly winds over the Barents Sea opening. This strength is related to the sea level pressure (SLP) gradient between the northern tip of Norway and Spitzbergen (Bengtsson et al., 2004). We therefore analyse the link between this SLP difference for JFM (that serves as an index of the winter oceanic inflow), the NAO and March SIA in the Barents Sea. As for the link between SIA and AMOC, correlations are computed for detrended time series for 1900–1970 and 2030–2100. The results are presented for interannual and decadal (5 year running means) variations.

3.7.1 Barents Sea SIA and NAO

Correlation between March SIA in the Barents Sea and the NAO index in CMIP3 and CMIP5-RCP 8.5 are shown in Fig. 12. The same type of presentation is used as for the correlations with the AMOC (Fig. 11). During the 20th century, basically all analysed models feature a negative correlation of the interannual SIA variability with the NAO index (Fig. 12a and b), with many exceeding the 5 % level of statistical significance (0.24). This demonstrates that most models are capable of, at least qualitatively, capturing the important dynamical link between the NAO and Barents Sea SIA. The negative correlation is also present during the 21st century. On the decadal time scale, the relation is in general stronger in both ensembles, but the spread becomes larger and several models that exhibit a significant correlation to the NAO during the 20th century show now much weaker or even positive correlations (Fig. 12c and d). This may in part be related to the fact that several models reach an ice free regime in the Barents Sea towards around 2050.

TCD
9, 1077–1131, 2015

3.7.2 Barents Sea SIA and SLP difference Scandinavia–Spitzbergen

The correlations of the March Barents Sea SIA with JFM SLP difference between Scandinavia and Spitsbergen, which serves here as an index of the oceanic inflow to the Barents Sea through its eastern opening, are presented in Fig. 13. Both ensembles generally show negative correlations on interannual timescales (Fig. 13a and b), which is expected as more warm Atlantic waters enter the inner Barents Sea thereby reducing sea ice area. There are no considerable differences between the 20th and 21st century results. Models that depict a stronger correlation in the 20th century tend to also have stronger correlation in the 21st century. The relation is somewhat weaker in CMIP5 ensemble. The results are similar for decadal timescales (Fig. 13c and d), although both ensembles exhibit a large spread. It should be kept in mind, however, that time series are rather short to study decadal variability in detail. The correlation changes its sign in a considerable portion of CMIP5 models when moving from the 20th century to the 21st century (Fig. 13d). This again may be related to the rather strong radiative forcing that causes sea ice to completely disappear in the Barents Sea in the middle of the 21st century (Fig. 4f). The analysis indicates that, despite the strongly overestimated SIA in the Barents Sea, many models simulate a significant impact of the oceanic inflow on SIA at interannual to decadal time scales.

4 Summary and conclusions

Arctic sea ice in models that participated in the Coupled Model Intercomparison Project Phase 3 and 5 (CMIP3 and CMIP5) has been analyzed. Sea ice concentration (SIC) variability patterns and their simulated future changes have been studied first. This was followed by the investigation of changes in sea ice area (SIA) in the Entire Arctic, Central Arctic and Barents Sea in March and September. Further, the SIA seasonal cycle amplitude, interannual variability and decadal variability have been investigated. We also investigated the sensitivity of SIA changes to Northern Hemisphere surface air

TCD
9, 1077–1131, 2015

temperature (SAT) and Atlantic Meridional Overturning Circulation (AMOC) and links between SIA variability and the AMOC, North Atlantic Oscillation (NAO) and sea level pressure (SLP) gradient between Scandinavia and Spitsbergen serving as an index of oceanic inflow to the Barents Sea. In the following, we provide an overview of major findings.

Our analyses for summer sea ice area (SIA) in the Entire Arctic are consistent with previous studies (Stroeve et al., 2007; Stoeve et al., 2012; Wang and Overland, 2009) which considered summer sea ice extent (SIE). Both model ensembles show a consistent SIA decline when forced by estimates of historical external forcing and future scenarios of anthropogenic greenhouse gases and aerosols. The CMIP5 models better reproduce both the mean state and observed long-term trend of the Entire Arctic SIA in September. In particular, the CMIP5 ensemble on average simulates a stronger decline which is more consistent with the observed SIA trend. The recent accelerated Arctic sea ice loss during the early the 21st century, however, is still not fully captured, which may suggest a contribution from internal variability, an underestimated sensitivity to the applied forcing and/or incomplete forcing. Many CMIP5 models exhibit a step like SIA decrease in the first half of the 21st century, resulting from a seasonally ice free Arctic around 2050 and possibly suggesting the existence of a "tipping point" in the Arctic climate system. A clear improvement in the simulation of September SIA in the Entire Arctic by the CMIP5 models during 1950–2010 is seen in comparison to CMIP3, but at the same time is is accompanied by larger biases for March SIA. Regional SIA changes are characterized by much stronger uncertainties that changes in the Entire Arctic. The models in both ensembles tend to strongly overestimate SIA in the Barents Sea in September (by a factor of 3 to 4) and exhibit a very large spread concerning mean state and trends. Many models depict large departures from the observations. SIA in individual runs (in all analysed regions) exhibits strong decadal variability in both March and September, which is consistent with the observed decadal variations seen at a regional scale and may also explain the accelerated sea ice retreat during the early 21st century.

TCD
9, 1077–1131, 2015

The pattern of SIC interannual variability in September is also improved in the CMIP5 models, with larger interannual variability than the CMIP3 models. However, the variability is still weaker than the observed, especially in the Atlantic sector. The model spread is also reduced in comparison to CMIP3. Much better simulation of the interannual variability along the Arctic sea ice margin is, however, accompanied by overestimated variability in large parts of the Central Arctic, suggesting an overall increase of sensitivity of summer SIC to heat balance variations at the atmosphere–ocean interface. In winter, the CMIP5 models also demonstrate a better agreement with observations, although not as much as in summer. In future projections, the CMIP5 models under the RCP 4.5 scenario exhibit a stronger variability increase in many regions in comparison to the CMIP3 models under the weaker SRES A1B scenario. This also suggests a higher sensitivity of SIC to greenhouse warming in the CMIP5 ensemble.

The dependence of SIA on NH SAT, when considering the Entire Arctic, is most robust in winter and of rather similar strength in the two model ensembles. In summer, the CMIP5 models when forced by the RCP 8.5 scenario show a considerably weaker link of SIA to SAT than the CMIP3 models (employing the SRES A1B scenario). This may be explained by the much stronger forcing creating, for the majority of models, an ice free Arctic during summer around 2050. For the Central Arctic, the CMIP5 (RCP 8.5) models also generally depict a weaker dependence of summer SIA on SAT than the CMIP3 models. For the Barents Sea, the dependence on SAT is the weakest, particularly in summer, indicating a large spread of the model results in this region. Overall, the large model spread implies a strong dependence of SIA on the hemispheric-scale SAT response to anthropogenic forcing and thus transient climate sensitivity.

The amplitude of the SIA seasonal cycle increases in the observations, as implied by the stronger decrease of SIA during September than that in March. This tendency is reproduced by the models in the Entire Arctic and Central Arctic, with stronger trends simulated by CMIP5 models (forced by RCP 8.5 scenario). However, both model ensembles overestimate the amplitude in comparison to the observations, with the CMIP5 models having, on average, a noticeably stronger positive bias in both the Entire Arctic

TCD
9, 1077–1131, 2015

and Central Arctic. The enhanced amplitude of the seasonal cycle along with lower SIA in all seasons results in a substantially increased (by about 50 %) seasonality of the Entire Arctic sea ice cover, especially in the CMIP5 models. The increase in the SIA seasonal cycle amplitude may also serve as a good indicator of the amount of newly formed ice during autumn and winter. Both model ensembles are characterized by very large uncertainties in the Barents Sea. Strong decadal to inter-decadal amplitude variability in the Barents Sea is simulated by the majority of models, consistent with observations and the notion that the Barents Sea is a region which is strongly affected by internal variability.

SIA interannual variability changes in the Entire Arctic have been estimated by comparing SIA SDs simulated during the 20th century with those during the 21st century. The CMIP3 models generally better reproduce the observed variability in March, but strongly underestimate it in September. The situation is the opposite in the CMIP5 models. Finally, in the second half of the 21st century, the number of CMIP3 models that simulate a stronger interannual variability in September relative to that in March considerably increases, whereas the majority of CMIP5 models predict a strong reduction of interannual SIA variability in both March and September.

The relation between SIA change and annual-mean AMOC change exhibits principally different behavior in March and September in both model ensembles. The stronger decrease in SIA in September is associated with stronger AMOC slowing, whereas stronger SIA reduction in March is accompanied by weaker AMOC slowing. This suggests that the long-term AMOC slowdown under global warming and associated poleward oceanic heat transport reduction plays a more important role in SIA change during winter than in summer. The link between SIA and AMOC changes is much stronger in the CMIP5 models, implying more prominent role of dynamical processes.

During the 20th century, most CMIP3 models simulate a negative correlation between AMOC and SIC variations in the Entire Artic, as well as for the Barents Sea. However, several models show a positive correlation during the 20th or 21st centuries,

TCD
9, 1077–1131, 2015

or both. The majority of CMIP5 models depict a negative correlation between AMOC and SIA variations in the Entire Arctic and Barents Sea, with roughly half of models changing the sign of the relationship. Thus, the models generally are capable to simulate a link between SIA and AMOC-related oceanic heat transport changes.

The models in both ensembles are capable of capturing the important dynamical link between the NAO and SIA in the Barents Sea. This relationship is generally unchanged in the 21st century. Despite strongly overestimated SIA in the Barents Sea, many models are also capable of simulating a link between the oceanic inflow to the Sea and SIA variations on interannual to decadal timescales. This indicates that dynamical processes related to natural oceanic and atmospheric variability do contribute to variations in the sea ice cover in the models. This may explain stronger differences from observations on decadal timescales.

We conclude that the models forced by increasing greenhouse gas concentrations simulate not only a coherent decline of the Arctic mean sea ice area, but also exhibit consistent changes of the seasonal cycle characteristics and spatial patterns of SIC interannual variability. A clear improvement in simulating the SIA in summer by the CMIP5 ensemble in comparison to CMIP3 models is often accompanied by worse results for winter SIA characteristics, including changes of the mean, seasonal cycle and interannual variability. Regional changes are characterized by much higher uncertainties than changes computed for the Entire Arctic. This is particularly the case for the Barents Sea ice which is strongly influenced by natural oceanic and atmospheric variability.

The high uncertainty and strong regional model biases are very important issues for the attribution of the recent climate and weather anomalies in the northern high latitudes to the Arctic sea ice changes (see Vihma, 2014 for review). Given a possible strongly-nonlinear circulation response to even present climate changes of the Arctic SIC and strong dependence on the mean state (Petoukhov and Semenov, 2010), analysis of the future circulation response based on CMIP models should be performed with caution.

TCD
9, 1077–1131, 2015

Acknowledgements. We acknowledge the World Climate Research Programme's Working Group on Coupled Modelling, which is responsible for CMIP, and we thank the climate modeling groups (listed in Table 1 and 2 of this paper) for producing and making available their model output. For CMIP the US Department of Energy's Program for Climate Model Diagnosis and Intercomparison (PCDMI) provides coordinating support and led development of software infrastructure in partnership with the Global Organization for Earth System Science Portals. This work was supported by the RACE Project of BMBF, the European Union's NACLIM and NordForsk GREENICE projects. Analysis of SIA variability in the Barents Sea was supported by Russian Science Foundation (grant no. 14-17-00647).

The service charges for this open-access publication have been covered by a Research Centre of the Helmholtz Association.

References

Alekseev, G. V., Kuzmina, S. I., Nagurny, A. P., and Ivanov, N. E.: Arctic Sea ice data sets in the context of climate change during the 20th century, climate variability and extremes during the past 100 years, Adv. Glob. Change Res., 33, 47–63, 2007.

Alekseev, G. V., Danilov, A. I., Kattsov, V. M., Kuz'mina, S. I., and Ivanov, N. E.: Changes in the climate and sea ice of the Northern Hemisphere in the 20th and 21st centuries from data of observations and modeling, Izvestiya, Atmos. Ocean. Phys., 45, 675–686, doi:10.1134/S0001433809060012, 2009.

Alexeev, V. A., Langen, P. L., and Bates, J. R.: Polar amplification of surface warming on an aquaplanet in "ghost forcing" experiments without sea ice feedbacks, Clim. Dynam., 24, 655–666, 2005.

Bengtsson, L., Semenov, V. A., and Johannessen, O. M.: The early twentieth-century warming in the Arctic – a possible mechanism, J. Climate, 17, 4045–4057, 2004.

Cavalieri, D. J. and Parkinson, C. L.: Arctic sea ice variability and trends, 1979–2010, The Cryosphere, 6, 881–889, doi:10.5194/tc-6-881-2012, 2012.

TCD
9, 1077–1131, 2015

Day, J. J., Hargreaves, J. C., Annan, J. D., and Abe-Ouchi, A.: Sources of multi-decadal variability in Arctic sea ice extent, Environ. Res. Lett., 7, 034011, doi:10.1088/1748-9326/7/3/034011, 2012.

Delworth, T. L. and Mann, M. E.: Observed and simulated multidecadal variability in the Northern Hemisphere, Clim. Dynam., 16, 661–676, 2000.

Dickson, R. R., Osborn, T. J., Hurrell, J. W., Meincke, J., Blindheim, J., Adlandsvik, B., Vinje, T., Alekseev, G., and Maslowski, W.: The Arctic Ocean response to the North Atlantic oscillation, J. Climate, 13, 2671–2696, 2000.

Divine, D. V. and Dick, C.: Historical variability of sea ice edge position in the Nordic Seas, J. Geophys. Res.-Oceans, 111, C01001, doi:10.1029/2004jc002851, 2006.

Eisenman, I., Untersteiner, N., and Wettlaufer, J. S.: On the reliability of simulated Arctic sea ice in global climate models, Geophys. Res. Lett., 34, L10501, doi:10.1029/2007GL029914, 2007.

Flato, G., Marotzke, J., Abiodun, B., Braconnot, P., Chou, S. C., Collins, W., Cox, P., Driouech, F., Emori, S., Eyring, V., Forest, C., Gleckler, P., Guilyardi, E., Jakob, C., Kattsov, V., Reason, C., and Rummukainen, M.: Evaluation of climate models, in: Climate Change 2013: The Physical Science Basis. Contribution of Working Group I to the Fifth Assessment Report of the Intergovernmental Panel on Climate Change, edited by: Stocker, T. F., Qin, D., Plattner, G.-K., Tignor, M., Allen, S. K., Boschung, J., Nauels, A., Xia, Y., Bex, V., and Midgley, P. M., Cambridge University Press, Cambridge, UK and New York, NY, USA, 2013.

Gloersen, P., Campbell, W. J., Cavalieri, D. J., Comiso, J. C., Parkinson, C. L., and Zwally, J. H.: Arctic and Antarctic Sea Ice, 1978–1987: Satellite Passive-Microwave Observations and Analysis, National Aeronautics and Space Administration, Washington, D.C., 1992.

Goosse, H., Arzel, O., Bitz, C. M., de Montety, A., and Vancoppenolle, M.: Increased variability of the Arctic summer ice area in a warmer climate, Geophys. Res. Lett., 36, L23702, doi:10.1029/2009GL040546, 2009.

Goosse, H. and Holland, M. M.: Mechanisms of decadal Arctic climate variability in the Community Climate System Model, Version 2 (CCSM2), J. Climate, 18, 3552–3570, 2005.

Granger, C. H. J. and Hatanaka, M.: Spectral Analysis of Economic Time Series, University Press Princeton, Princeton, NJ, 1964.

Graversen, R. G., Mauritsen, T., Tjernstrom, M., Kallen, E., and Svensson, G.: Vertical structure of recent Arctic warming, Nature, 451, 53–56, 2008.

TCD
9, 1077–1131, 2015

Guo, D., Gao, Y., Bethke, I., Gong, D., Johannessen, O. M., and Wang, H.: Mechanism on how the spring Arctic sea ice impacts the East Asian summer monsoon, Theor. Appl. Climatol., 115, 107–119, doi:10.1007/s00704-013-0872-6, 2013.
Halfar, J., Adey, W. H., Kronz, A., Hetzinger, S., Edinger, E., and Fitzhugh, W. W.: Arctic sea-ice decline archived by multicentury annual-resolution record from crustose coralline algal proxy, P. Natl. Acad. Sci. USA, 110, 19737–19741, doi:10.1073/pnas.1313775110, 2014.
Hodson, D. L. R., Keeley, S. P. E., West, A., Ridley, J., Hawkins, E., and Hewitt, H. T.: Identifying uncertainties in Arctic climate change projections, Clim. Dynam., 40, 2849–2865, doi:10.1007/s00382-012-1512-z, 2013.
Holland, M. M. and Bitz, C. M.: Polar amplification of climate change in coupled models, Clim. Dynam., 21, 221–232, 2003.
Holland, M. M. and Stroeve, J.: Changing seasonal sea ice predictor relationships in a changing Arctic climate, Geophys. Res. Lett., 38, 1–6, doi:10.1029/2011GL049303, 2011.
Holland, M. M., Bitz, C. M., Tremblay, L., and Bailey, D. A.: The role of natural versus forced change in future rapid summer Arctic ice loss, Arctic Sea ice decline: observations, projections, mechanisms, and implications, Geoph. Monog. Series, 180, 133–150, 2008.
Hurrell, J. W.: Decadal trends in the North-Atlantic oscillation – regional temperatures and precipitation, Science, 269, 676–679, 1995.
Inoue, J., Hori, M. E., and Takaya, K.: The role of Barents Sea ice in the wintertime cyclone track and emergence of a warm-arctic cold-siberian anomaly, J. Climate, 25, 2561–2568, 2012.
Ivanova, N., Johannessen, O. M., Pedersen, L. T., and Tonboe, R. T.: Retrieval of Arctic sea ice parameters by satellite passive microwave sensors: a comparison of eleven sea ice algorithms, IEEE T. Geosci. Remote, 52, 7233–7246, doi:10.1109/TGRS.2014.2310136, 2014.
IPCC: Climate Change 2007: The Physical Science Basis – Contribution of Working Group I to the Fourth Assessment Report, 15 IPCC Model Documentation: CMIP3 climate model documentation, references, and links, Intergovernmental Panel on Climate Change, available at: http://www-pcmdi.llnl.gov/ipcc/model_documentation/ipcc_model_documentation.php (last access: 18 February 2015), Cambridge University Press, Cambridge, 2007.
IPCC: Climate Change 2013: The Physical Science Basis. Contribution of Working Group I to the Fifth Assessment Report of the Intergovernmental Panel on Climate Change, edited by: Stocker, T. F., Qin, D., Plattner, G.-K., Tignor, M., Allen, S. K., Boschung, J., Nauels, A.,

TCD
9, 1077–1131, 2015

Xia, Y., Bex, V., and Midgley, P. M., Cambridge University Press, Cambridge, UK and New York, NY, USA, 1535 pp., doi:10.1017/CBO9781107415324, 2013.
Johannessen, O. M., Bengtsson, L., Miles, M. W., Kuzmina, S. I., Semenov, V. A., Alekseev, G. V., Nagurnyi, A. P., Zakharov, V. F., Bobylev, L. P., Pettersson, L. H., Hasselmann, K., and Cattle, A. P.: Arctic climate change: observed and modelled temperature and sea-ice variability, Tellus A, 56, 328–341, 2004.
Jungclaus, J. H. and Koenigk, T.: Low-frequency variability of the arctic climate: the role of oceanic and atmospheric heat transport variations, Clim. Dynam., 34, 265–279, doi:10.1007/s00382-009-0569-9, 2010.
Jungclaus, J. H., Haak, H., Latif, M., and Mikolajewicz, U.: Arctic-North Atlantic interactions and multidecadal variability of the meridional overturning circulation, J. Climate, 18, 4013–4031, 2005.
Karlsson, J. and Svensson, G.: Consequences of poor representation of Arctic sea-ice albedo and cloud-radiation interactions in the CMIP5 model ensemble, Geophys. Res. Lett., 40, 4374–4379, doi:10.1002/grl.50768, 2013.
Kattsov, V. M., Ryabinin, V. E., Overland, J. E., Serreze, M. C., Visbeck, M., Walsh, J. E., Meier, W., and Zhang, X.: Arctic sea-ice change: a grand challenge of climate science, J. Glaciol., 56, 1115–1121, 2010.
Khon, V. C., Mokhov, I. I., Latif, M., Semenov, V. A., and Park, W.: Perspectives of Northern sea route and Northwest Passage in the 21st century, Clim. Change, 100, 757–768, doi:10.1007/s10584-009-9683-2, 2010.
Kinnard, C., Zdanowicz, C. M., Fisher, D. A., Isaksson, E., de Vernal, A, and Thompson, L. G.: Reconstructed changes in Arctic sea ice over the past 1450 years, Nature, 479, 509–512, 2011.
Koenigk, T., Devasthale, A., and Karlsson, K.-G.: Summer Arctic sea ice albedo in CMIP5 models, Atmos. Chem. Phys., 14, 1987–1998, doi:10.5194/acp-14-1987-2014, 2014.
Kravtsov, S. and Spannagle, C.: Multidecadal climate variability in observed and modeled surface temperatures, J. Climate, 21, 1104–1121, doi:10.1175/2007jcli1874.1, 2008.
Kuzmina, S. I., Bengtsson, L., Johannessen, O. M., Drange, H., Bobylev, L. P., and Miles, M. W.: The North Atlantic Oscillation and greenhouse-gas forcing, Geophys. Res. Lett., 32, L04703, doi:10.1029/2004gl021064, 2005.
Kwok, R.: Recent changes in Arctic Ocean sea ice motion associated with the North Atlantic Oscillation, Geophys. Res. Lett., 27, 775–778, 2000.

TCD
9, 1077–1131, 2015

Latif, M., Roeckner, E., Botzet, M., Esch, M., Haak, H., Hagemann, S., Jungclaus, J., Legutke, S., Marsland, S., Mikolajewicz, U., and Mitchell, J.: Reconstructing, monitoring, and predicting multidecadal-scale changes in the North Atlantic thermohaline circulation with sea surface temperature, J. Climate, 17, 1605–1614, 2004.

Lenton, T. M., Held, H., Kriegler, E., Hall, J. W., Lucht, W., Rahmstorf, S., and Schellnhuber, H. J.: Tipping elements in the Earth's climate system, P. Natl. Acad. Sci. USA, 105, 1786–1793, doi:10.1073/pnas.0705414105, 2008.

Mahajan, S., Zhang, R., and Delworth, T. L.: Impact of the Atlantic Meridional Overturning Circulation (AMOC) on Arctic surface air temperature and sea ice variability, J. Climate, 24, 6573–6581, doi:10.1175/2011jcli4002.1, 2012.

Massonnet, F., Fichefet, T., Goosse, H., Bitz, C. M., Philippon-Berthier, G., Holland, M. M., and Barriat, P.-Y.: Constraining projections of summer Arctic sea ice, The Cryosphere, 6, 1383–1394, doi:10.5194/tc-6-1383-2012, 2012.

Mauritsen, T., Stevens, B., Roeckner, E., Crueger, T., Esch, M., Giorgetta, M., Haak, H., Jungclaus, J., Klocke, D., Matei, D., Mikolajewicz, U., Notz, D., Pincus, R., Schmidt, H., and Tomassini, L.: Tuning the climate of a global model, J. Adv. Model. Earth Syst., 4, M00A01, doi:10.1029/2012MS000154, 2012.

Meehl, G. A., Covey, C., Delworth, T., Latif, M., McAvaney, B., Mitchell, J. F. B., Stouffer, R. J., and Taylor, K. E.: The WCRP CMIP3 multimodel dataset – A new era in climate change research, B. Am. Meteorol. Soc., 88, 1383–1394, doi:10.1175/bams-88-9-1383, 2007.

Mahlstein, I. and Knutti, R.: September Arctic sea ice predicted to disappear near 2 degrees C global warming above present, J. Geophys. Res.-Atmos., 117, D06104, doi:10.1029/2011jd016709, 2011.

Meinshausen, M., Smith, S. J., Calvin, K., Daniel, J. S., Kainuma, M. L. T., Lamarque, J. F., Matsumoto, K., Montzka, S. A., Raper, S. C. B., Riahi, K., Thomson, A., Velders, G. J. M., and van Vuuren, D. P. P.: The RCP greenhouse gas concentrations and their extensions from 1765 to 2300, Clim. Change, 109, 213–241, doi:10.1007/s10584-011-0156-z, 2011.

Miles, M. W., Divine, D. V., Furevik, T., Jansen, E., Moros, M., and Ogilvie, A. E. J.: A signal of persistent Atlantic multidecadal variability in Arctic sea ice, Geophys. Res. Lett., 41, 463–469, doi:10.1002/2013GL058084, 2014.

Mysak, L. A. and Venegas, S. A.: Decadal climate oscillations in the Arctic: a new feedback loop for atmosphere–ice–ocean interactions, Geophys. Res. Lett., 25, 3607–3610, 1998.

TCD
9, 1077–1131, 2015

Notz, D. and Marotzke, J.: Observations reveal external driver for Arctic sea-ice retreat, Geophys. Res. Lett., 39, L08502, doi:10.1029/2012gl051094, 2012.
Overland, J. E., Adams, J. M., and Bond, N. A.: Regional variation of winter temperatures in the Arctic, J. Climate, 10, 821–837, 1997.
Peings, Y. and Magnusdottir, G.: Forcing of the wintertime atmospheric circulation by the multidecadal fluctuations of the North Atlantic ocean, Environ. Res. Lett., 9, 034018, doi:10.1088/1748-9326/9/3/034018, 2014.
Petoukhov, V. and Semenov, V. A.: A link between reduced Barents-Kara sea ice and cold winter extremes over northern continents, J. Geophys. Res., 115, 1–11, doi:10.1029/2009JD013568, 2010.
Polyakov, I. V., Alekseev, G. V., Bekryaev, R. V., Bhatt, U. S., Colony, R., Johnson, M. A., Karklin, V. P., Walsh, D., and Yulin, A. V.: Long-term ice variability in Arctic marginal seas, J. Climate, 16, 2078–2085, 2003.
Polyakov, I. V., Alexeev, V. A., Bhatt, U. S., Polyakova, E. I., and Zhang, X. D.: North Atlantic warming: patterns of long-term trend and multidecadal variability, Clim. Dynam., 34, 439–457, doi:10.1007/s00382-008-0522-3, 2010.
Rayner, N. A.: Global analyses of sea surface temperature, sea ice, and night marine air temperature since the late nineteenth century, J. Geophys. Res., 108, 4407, doi:10.1029/2002JD002670, 2003.
Rogers, T. S., Walsh, J. E., Rupp, T. S., Brigham, L. W., and Sfraga, M.: Future Arctic marine access: analysis and evaluation of observations, models, and projections of sea ice, The Cryosphere, 7, 321–332, doi:10.5194/tc-7-321-2013, 2013.
Schneider, B., Latif, M., and Schmittner, A.: Evaluation of different methods to assess model projections of the future evolution of the Atlantic meridional overturning circulation, J. Climate, 20, 2121–2132, doi:10.1175/jcli4128.1, 2007.
Screen, J. A.: Influence of Arctic sea ice on European summer precipitation, Environ. Res. Lett., 8, 044015, doi:10.1088/1748-9326/8/4/044015, 2013.
Screen, J. A. and Simmonds, I.: The central role of diminishing sea ice in recent Arctic temperature amplification, Nature, 464, 1334–1337, 2010.
Schweiger, A., Lindsay, R., Zhang, J., Steele, M., Stern, H., and Kwok, R.: Uncertainty in modeled Arctic Sea ice volume, J. Geophys. Res., 116, C00D06, doi:10.1029/2011JC007084, 2011.

TCD
9, 1077–1131, 2015

Semenov, V. A.: Influence of oceanic inflow to the Barents Sea on climate variability in the Arctic region, Dokl. Earth Sci., 418, 91–94, doi:10.1134/S1028334X08010200, 2008.
Semenov, V. A. and Bengtsson, L.: Modes of the wintertime Arctic temperature variability, Geophys. Res. Lett., 30, 1781, doi:10.1029/2003GL017112, 2003.
Semenov, V. A. and Latif, M.: The early twentieth century warming and winter Arctic sea ice, The Cryosphere, 6, 1231–1237, doi:10.5194/tc-6-1231-2012, 2012.
Semenov, V. A., Latif, M., Jungclaus, J. H., and Park, W.: Is the observed NAO variability during the instrumental record unusual?, Geophys. Res. Lett., 35, L11701, doi:10.1029/2008gl033273, 2008.
Semenov, V. A., Park, W., and Latif, M.: Barents Sea inflow shutdown: a new mechanism for climate changes, Geophys. Res. Lett., 36, L14709, doi:10.1029/2009GL038911, 2009.
Semenov, V. A., Latif, M., Dommenget, D., Keenlyside, N. S., Strehz, A., Martin, T., and Park, W.: The impact of North Atlantic-Arctic multidecadal variability on Northern Hemisphere surface air temperature, J. Climate, 23, 5668–5677, doi:10.1175/2010jcli3347.1, 2010.
Serreze, M. C., Barrett, A. P., Stroeve, J. C., Kindig, D. N., and Holland, M. M.: The emergence of surface-based Arctic amplification, The Cryosphere, 3, 11–19, doi:10.5194/tc-3-11-2009, 2009.
Smedsrud, L. H., Esau, I., Ingvaldsen, R. B., Eldevik, T., Haugan, P. M., Li, C., Lien, V. S., Olsen, A., Omar, A. M., Ottera, O. H., Risebrobakken, B., Sando, A. B., Semenov, V. A., and Sorokina, S. A.: The role of the Barents Sea in the Arctic climate system, Rev. Geophys., 51, 415–449, doi:10.1002/rog.20017, 2013.
Stroeve, J., Holland, M. M., Meier, W., Scambos, T., and Serreze, M.: Arctic sea ice decline: faster than forecast, Geophys. Res. Lett., 34, 1–5, doi:10.1029/2007GL029703, 2007.
Stroeve, J. C., Kattsov, V., Barrett, A., Serreze, M., Pavlova, T., Holland, M., and Meier, W. N.: Trends in Arctic sea ice extent from CMIP5, CMIP3 and observations, Geophys. Res. Lett., 39, L16502, doi:10.1029/2012GL052676, 2012.
Tang, Q., Zhang., X., Yang, X., and Francis, J. A.: Cold winter extremes in northern continents linked to Arctic sea ice loss, Environ. Res. Lett., 8, 014036, doi:10.1088/1748-9326/8/1/014036, 2013.
Taylor, K. E., Stouffer, R. J., and Meehl, G. A.: An Overview of CMIP5 and the experiment design, B. Am. Meteorol. Soc., 93, 485–498, doi:10.1175/BAMS-D-11-00094.1, 2012.

TCD
9, 1077–1131, 2015

Trenberth, K. E. and Caron, J. M.: Estimates of meridional atmosphere and ocean heat transports, J. Climate, 14, 3433–3443, doi:10.1175/1520-0442(2001)014<3433:EOMAAO>2.0.CO;2, 2001.
van Loon, H. and Rogers, J.: The seesaw in winter temperature between Greenland and northern Europe, Part I: General description, Mon. Weather Rev., 106, 296–310, 1978.
Vaughan, D. G., Comiso, J. C., Allison, I., Carrasco, J., Kaser, G., Kwok, R., Mote, P., Murray, T., Paul, F., Ren, J., Rignot, E., Solomina, O., Steffen, K., and Zhang, T.: Observations: cryosphere, in: Climate Change 2013: The Physical Science Basis. Contribution of Working Group I to the Fifth Assessment Report of the Intergovernmental Panel on Climate Change, edited by: Stocker, T. F., Qin, D., Plattner, G.-K., Tignor, M., Allen, S. K., Boschung, J., Nauels, A., Xia, Y., Bex, V., and Midgley, P. M., Cambridge University Press, Cambridge, UK and New York, NY, USA, 2013.
Venegas, S. A. and Mysak, L. A.: Is there a dominant timescale of natural climate variability in the Arctic?, J. Climate, 13, 3412–3434, 2000.
Vihma, T.: Effects of Arctic Sea ice decline on weather and climate: a review, Surv. Geophys., 35, 1175–1214, doi:10.1007/s10712-014-9284-0, 2014.
Walsh, J. E.: Intensified warming of the Arctic: causes and impacts on middle latitudes, Global Planet. Change, 117, 52–63, 2014.
Walsh, J. E. and Chapman, W. L.: 20th-century sea-ice variations from observational data, edited by: Jeffries, M. O. and Eicken, H., Ann. Glaciol., 33, 444–448, 2001.
Walsh, J. E. and Johnson, C. M.: Analysis of Arctic sea ice fluctuations, 1953–77, J. Phys. Oceanogr., 9, 580–591, 1979.
Wang, M. and Overland, J. E.: A sea ice free summer Arctic within 30 years?, Geophys. Res. Lett., 36, L07502, doi:10.1029/2009GL037820, 2009.
Winton, M.: Do climate models underestimate the sensitivity of Northern Hemisphere sea ice cover?, J. Climate, 24, 3924–3934, doi:10.1175/2011jcli4146.1, 2011.
Wunsch, C.: The interpretation of short climate records, with comments on the North Atlantic and Southern Oscillations, B. Am. Meteorol. Soc., 80, 245–255, doi:10.1175/1520-0477(1999)080<0245:tioscr>2.0.co;2, 1999.
Yang, S. and Christensen, J. H.: Arctic sea ice reduction and European cold winters in CMIP5 climate change experiments, Geophys. Res. Lett., 39, L20707, doi:10.1029/2012gl053338, 2012.

TCD
9, 1077–1131, 2015

Zhang, X.: Sensitivity of arctic summer sea ice coverage to global warming forcing: towards reducing uncertainty in arctic climate change projections, Tellus A, 62, 220–227, doi:10.1111/j.1600-0870.2010.00441.x, 2010.

TCD
9, 1077–1131, 2015

Table 1. CMIP3 models used for the analysis. Models marked with * do not resolve smaller islands like Svalbard. Only models marked with [1] have preindustrial control runs included.

Model		Resolution Atmosphere	Resolution Ice
BCCR-BCM2.0[1]	Bjerknes Centre for Climate Research, Norway	T63 (~ 1.9° × 1.9°)	1° × 1°
CCCMA-CGCM3.1(T47)[1]	Canadian Centre for Climate Modelling and Analysis, Canada	T47 (~ 2.8° × 2.8°)	~ 3.7° × 3.75°
CCCMA-CGCM3.1(T63)[1]	Canadian Centre for Climate Modelling and Analysis, Canada	T63 (~ 1.9° × 1.9°)	~ 2.7° × 2.8125°
CNRM-CM3[1]	Centre National de Recherches Meteorologiques, France	T63 (~ 1.9° × 1.9°)	1° × 2°
CSIRO-Mk3.0[1]	Commonwealth Scientific and Industrial Research Organisation, Australia	T63 (~ 1.9° × 1.9°)	~ 1.8° × 1.875°
CSIRO-Mk3.5[1]	Commonwealth Scientific and Industrial Research Organisation, Australia	T63 (~ 1.9° × 1.9°)	~ 1.8° × 1.875°
GFDL-CM2.0	Geophysical Fluid Dynamics Laboratory, USA	2.0° × 2.5°	0.3° – 1° × 1°
GFDL-CM2.1[1]	Geophysical Fluid Dynamics Laboratory, USA	3° × 4°	0.3° – 1° × 1°
GISS-AOM[1]	Goddard Institute for Space Studies, USA	4° × 5°	3° × 4°
GISS-MODEL-E-R[1]	Goddard Institute for Space Studies, USA	4° × 5°	2° – 4° × 5°
INM-CM3.0[1]	Institute for Numerical Mathematics, Russia	4° × 5°	2° × 2.5°
IPSL-CM4[1]	Institut Pierre Simon Laplace, France	2.5° × 3.75°	2° × 1°
MIROC3.2(hires)[1,*]	Center for Climate System Research, Japan	T106 (~ 1.1° × 1.1°)	~ 0.5° × 1.125°
MIROC3.2(medres)[1,*]	Center for Climate System Research, Japan	T42 (~ 2.8° × 2.8°)	1° × 1°
MPI-ECHAM5	Max Planck Institut for Meteorology, Germany	T63 (~ 1.9° × 1.9°)	1° × 1°
MRI-CGCM2.3.2A[1]	Meteorological Research Institute, Japan	T42 (~ 2.8° × 2.8°)	0.5° – 2° × 2.5°
NCAR-CCSM3.0[1]	National Center for Atmospheric Research, USA	T85 (1.4° × 1.4°)	0.09° – 0.5° × 1.125°
UKMO-HadCM3*	Hadley Centre for Climate Prediction and Research/Met Office, UK	2.5° × 3.75°	1.25° × 1.25°
UKMO-HadGEM1	Hadley Centre for Climate Prediction and Research/Met Office, UK	~ 1.3° × 1.9°	0.09° – 1° × 1°

TCD
9, 1077–1131, 2015

Table 2. CMIP5 models used for the analysis.

Model		Resolution Atmosphere	Resolution Ice
ACCESS1-0	Commonwealth Scientific and Industrial Research Organisation and Bureau of Meteorology, Australia	1.875° × ~ 1.25	1° × 0.6°
ACCESS1-3	Commonwealth Scientific and Industrial Research Organisation and Bureau of Meteorology, Australia	1.875° × ~ 1.25	1° × 0.6°
BCC-CSM1-1-M	Beijing Climate Center, Meteorological Administration, China	1.125° × 1.125°	1° × ~ 0.8°
BCC-CSM1-1	Beijing Climate Center, Meteorological Administration, China	T42 (2.815° × 2.815°)	1° × ~ 0.8°
BNU-ESM	Beijing Normal University, China	T42 (2.8125° × 2.8125°)	1° × 0.9°
CCSM4	National Center for Atmospheric Research, USA	1.25° × ~ 0.9°	1.125° × ~ 0.5°
CESM1-BGC	National Center for Atmospheric Research, USA	1.25° × ~ 0.9°	1.125° × ~ 0.5°
CESM1-CAM5	National Center for Atmospheric Research, USA	1.25° × ~ 0.9°	1.125° × ~ 0.5°
CMCC-CMS	Centro Euro-Mediterraneo per i Cambiamenti Climatici, Italy	T63 (1.875° × 1.875°)	~ 1.98° × ~ 1.2°
CMCC-CM	Centro Euro-Mediterraneo per i Cambiamenti Climatici, Italy	T159 (0.75° × 0.75°)	~ 1.98° × ~ 1.2°
CNRM-CM5	Centre National de Recherches Meteorologiques, France	TL127 (1.4° × 1.4°)	~ 1° × 0.6°
CSIRO-Mk3-6-0	Centre National de Recherches Meteorologiques, France	T63 (1.9° × 1.9°)	1.9° × ~ 0.95°
CanESM2	Canadian Centre for Climate Modelling and Analysis, Canada	T63 (~ 2.8 × 2.8)	~ 1.4° × ~ 0.9
FGOALS-s2	Institute of Atmospheric Physics, Chinese Academy of Sciences, and Tsinghua University, China	2.8125° × 1.67°	1° × ~ 0.9°
GFDL-CM3	NOAA GFDL(201 Forrestal Rd, Princeton, NJ, 08540)	2.5° × 2°	1° × 0.9°
GFDL-ESM2G	NOAA GFDL(201 Forrestal Rd, Princeton, NJ, 08540)	2.5° × 2°	1° × ~ 0.86°
GFDL-ESM2M	NOAA GFDL(201 Forrestal Rd, Princeton, NJ, 08540)	2.5° × 2°	1° × 0.9°

TCD
9, 1077–1131, 2015

Table 2. Continued.

Model		Resolution Atmosphere	Resolution Ice
GISS-E2-H-CC	Goddard Institute for Space Studies, USA	2.5° × 2°	2.5° × 2°
GISS-E2-H	Goddard Institute for Space Studies, USA	2.5° × 2°	2.5° × 2°
GISS-E2-R-CC	Goddard Institute for Space Studies, USA	2.5° × 2°	1.25° × 1°
GISS-E2-R	Goddard Institute for Space Studies, USA	2.5° × 2°	1.25° × 1°
HadGEM2-AO	National Institute of Meteorological Research, South Korea	1.875° × ~ 1.24°	1° × ~ 0.8°
HadGEM2-CC	Met Office Hadley Centre, UK	1.875° × ~ 1.24°	1° × ~ 0.8°
HadGEM2-ES	Met Office Hadley Centre, UK	1.875° × ~ 1.24°	1° × ~ 0.8°
INMCM4	Institute for Numerical Mathematics, Russia	2° × 1.5°	1° × 0.53°
IPSL-CM5A-LR	Institut Pierre Simon Laplace, Paris, France	3.75° × 1.875°	~ 1.98° × ~ 1.21°
IPSL-CM5B-LR	Institut Pierre Simon Laplace, Paris, France	3.75° × 1.875°	~ 1.98° × ~ 1.21°
MIROC-ESM-CHEM	Japan Agency for Marine-Earth Science and Technology, AORI (Atmosphere and Ocean Research Institute, The University of Tokyo and National Institute for Environmental Studies, Japan	T42 (2.8125° × 2.8125°)	~ 1.41° × ~ 0.94°
MIROC-ESM	Japan Agency for Marine-Earth Science and Technology, AORI (Atmosphere and Ocean Research Institute, The University of Tokyo and National Institute for Environmental Studies, Japan	T42 (2.8125° × 2.8125°)	~ 1.41° × ~ 0.94°
MIROC5	Atmosphere and Ocean Research Institute, The University of Tokyo, National Institute for Environmental Studies and Japan Agency for Marine-Earth Science and Technology, Japan	T85 (~ 1.4° × ~ 1.4°)	~ 1.41° × ~ 0.8°
MPI-ESM-LR	Max Planck Institute for Meteorology, Germany	T63 (1.875° × 1.875°)	~ 1.41° × 0.82°
MPI-ESM-MR	Max Planck Institute for Meteorology, Germany	T63 (1.875° × 1.875°)	~ 0.45° × ~ 0.45°
MRI-CGCM3	Meteorological Research Institute, Japan	TL159 (1.125° × 1.125°)	1° × ~ 0.49°
MRI-ESM1	Norwegian Climate Centre, Norway	TL159 (1.125° × 1.125°)	1° × ~ 0.5°
NorESM1-ME	Norwegian Climate Centre, Norway	2.5° × 1.875°	1.125° × ~ 0.47°
NorESM1-M	Norwegian Climate Centre, Norway	2.5° × 1.875°	1.125° × ~ 0.47°

TCD
9, 1077–1131, 2015

Table 3. Sensitivity of the Entire Arctic sea ice area to Northern Hemisphere surface air temperature (SAT) in CMIP model ensembles as a ratio between SIA and SAT changes averaged over the periods 1970–2000 and 2070–2100. Presented are the slope of a linear regression in $10^6\,km^2\,°C^{-1}$ and the correlation coefficient (in brackets) for corresponding model ensembles (see Figs. 6 and 7).

	Winter			Summer		
	CMIP3 SRES A1B	CMIP5 RCP 4.5	CMIP5 RC P8.5	CMIP3 SRES A1B	CMIP5 RCP 4.5	CMIP5 RCP 8.5
	$10^6\,km^2\,°C^{-1}$					
Entire Arctic	−1.9 (−0.85)	−1.3 (−0.76)	−1.6 (−0.75)	−1.0 (−0.57)	−1.3 (−0.73)	−0.6 (−0.46)
Central Arctic	−0.2 (−0.60)	−0.1 (−0.64)	−0.4 (−0.71)	−0.7 (−0.66)	−0.5 (−0.56)	−0.2 (−0.35)
Barents Sea	−0.2 (−0.64)	−0.3 (−0.64)	−0.1 (−0.38)	0.6 (0.21)	−0.01 (−0.03)	0.01 (0.04)

TCD
9, 1077–1131, 2015

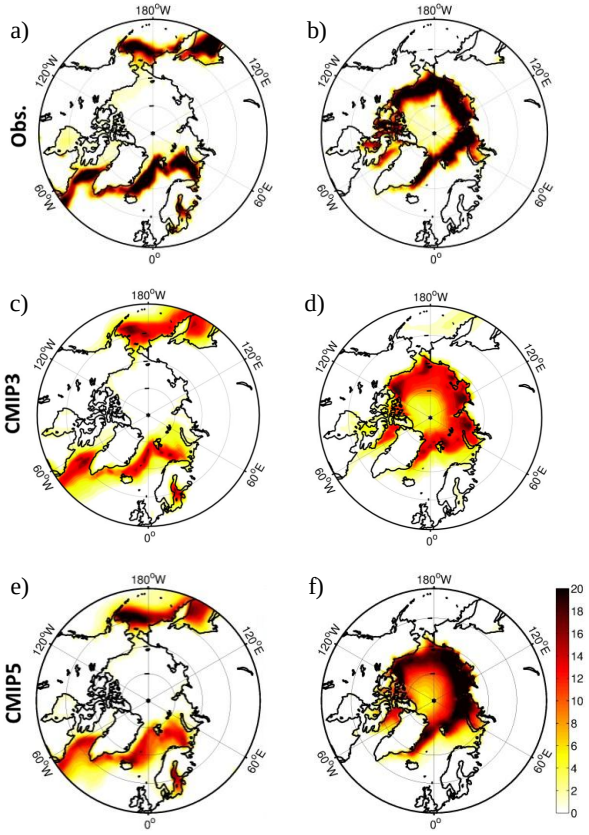

Figure 1. SD of interannual sea ice concentration (SIC) variability (in %) in March (left) and September (right) during 1950–2000 as estimated from historical observational data (HadISST1) **(a, b)**, CMIP3 (ensemble average; **c**, **d**), and CMIP5 (ensemble average; **e**, **f**). The CMIP results are from historical simulations. The long-term trend was removed from all datasets before estimating the SDs.

TCD
9, 1077–1131, 2015

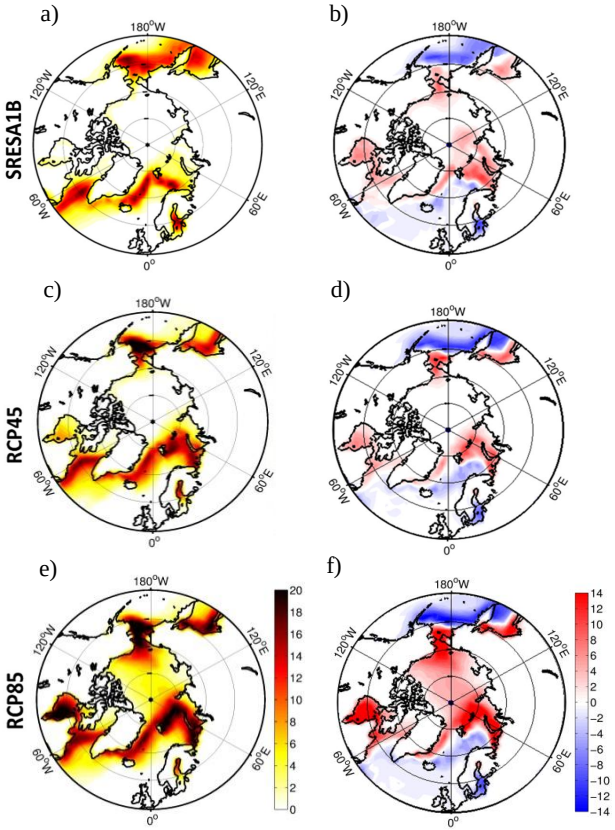

Figure 2. SD of interannual sea ice concentration (SIC) variability during 2050–2100 in March (% of concentration) in CMIP3-A1B **(a)** and CMIP5 (RCP 4.5, **c**; and RCP 8.5, **e**). Difference between SD during 2050–2100 and 1950–2000 for CMIP3-A1B **(b)** and CMIP5 (RCP 4.5, **d**; and RCP 8.5, **f**). The SDs have been computed for detrended data.

TCD
9, 1077–1131, 2015

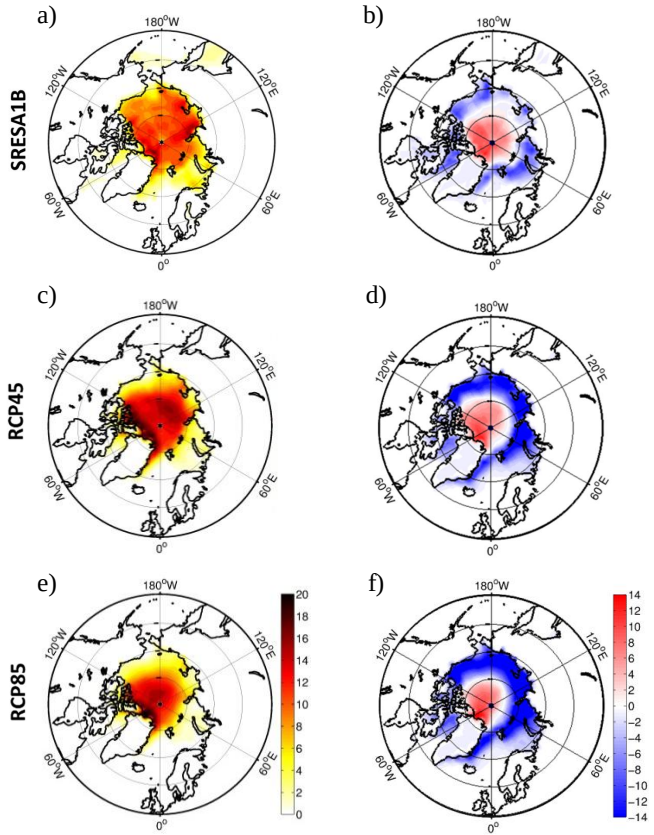

Figure 3. Same as in Fig. 2 but for September.

TCD
9, 1077–1131, 2015

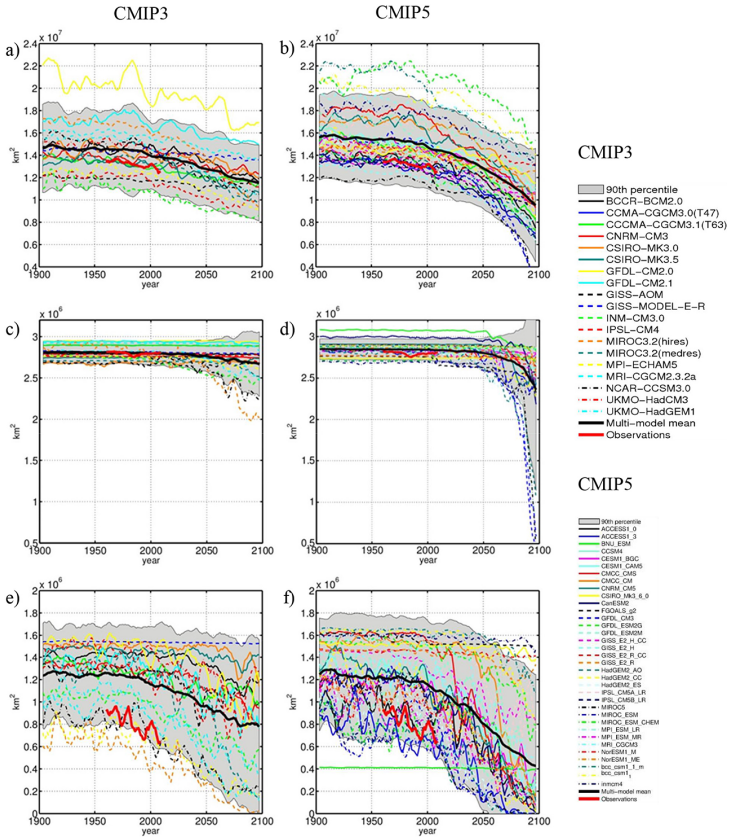

Figure 4. Time series of the sea ice area (SIA) for March (km^2) as observed (thick red) and simulated by CMIP3-A1B (left) and CMIP5-RCP 8.5 (right) models (thin colored) for the Entire Arctic **(a, b)**, Central Arctic **(c, d)**, and Barents Sea **(e, f)**. Time series are smoothed with a five year running mean. The thick black lines represent the multi-model mean. Grey shading depicts the 90 % confidence intervals estimated from the SD of the intra-ensemble spread.

TCD
9, 1077–1131, 2015

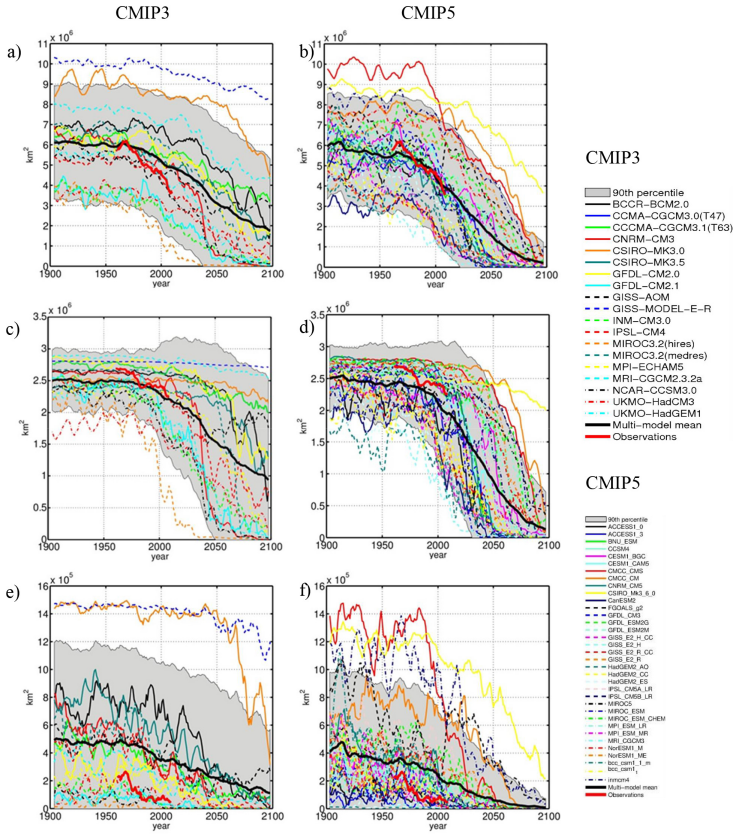

Figure 5. Same as in Fig. 4 but for September.

TCD
9, 1077–1131, 2015

Arctic sea ice area in CMIP3 and CMIP5 climate model ensembles

V. A. Semenov et al.

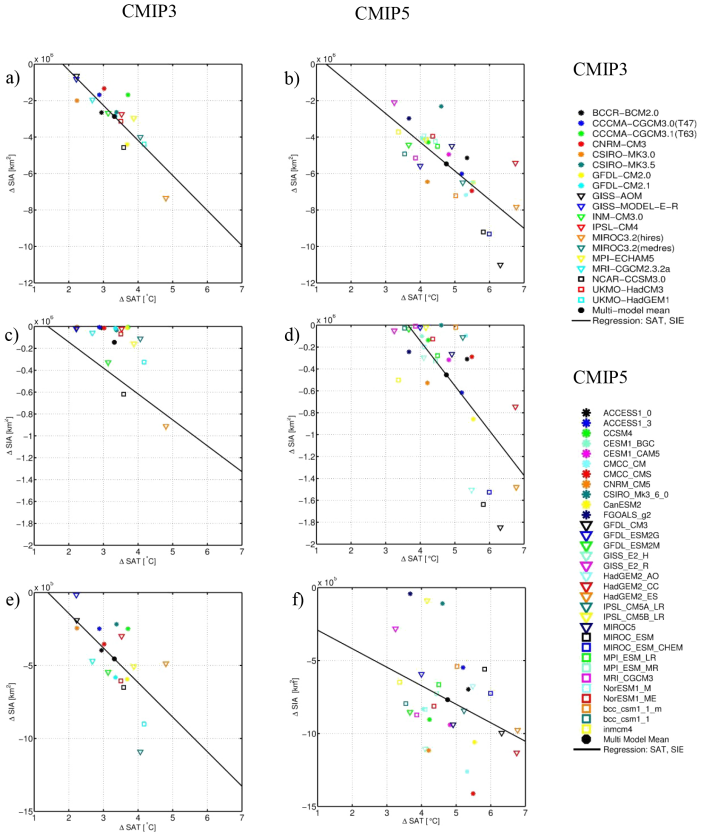

Figure 6. Sensitivity of sea ice area (SIA) to changes in Northern Hemisphere (NH) surface air temperature (SAT) between 1970–2000 and 2070–2100 in winter (January, February and March) for CMIP3 (20C3M/SRES A1b, left) and CMIP5 (historical/RCP 8.5, right). Shown are results for the Entire Arctic **(a, b)**, Central Arctic **(c, d)**, and Barents Sea **(e, f)**. Corresponding regression and correlation values are shown in Table 3.

TCD
9, 1077–1131, 2015

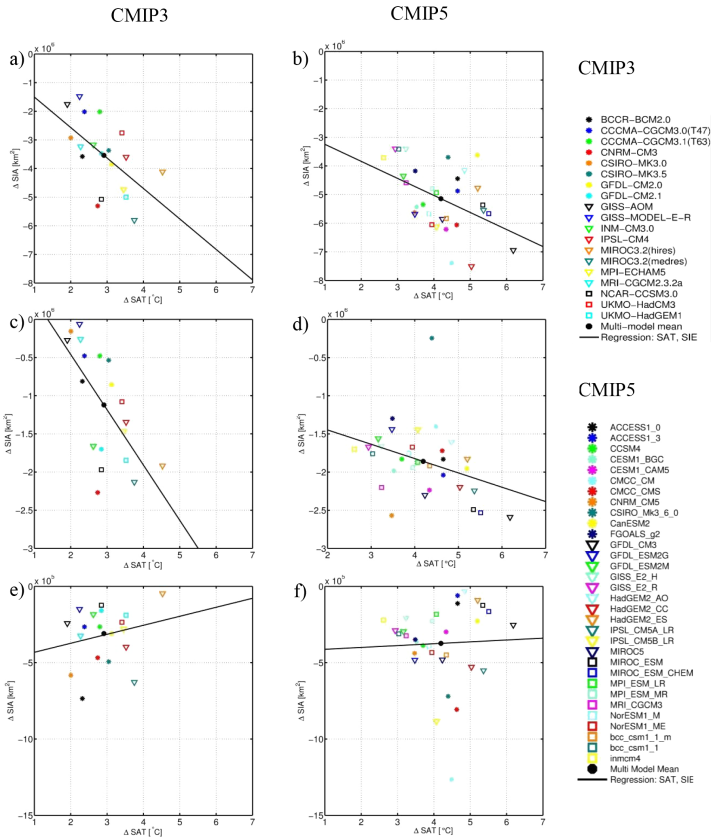

Figure 7. Same as in Fig. 6 but for summer (July, August and September).

TCD
9, 1077–1131, 2015

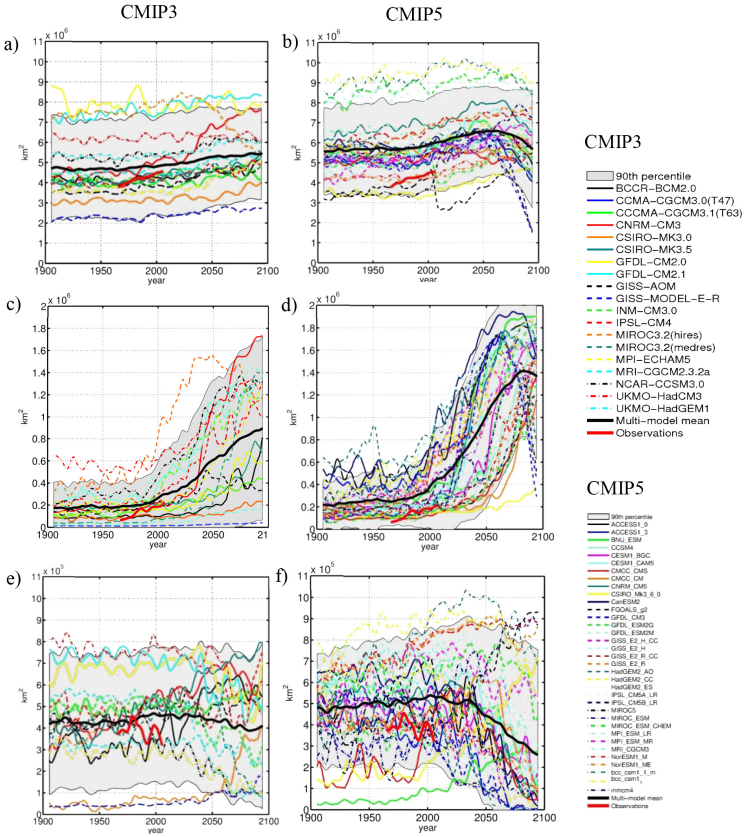

Figure 8. The amplitude of the sea ice area (SIA) seasonal cycle as estimated from observations (thick red) and the CMIP3 (left) and CMIP5 (right) ensembles (thin colored). Shown are the results for the Entire Arctic **(a, b)**, Central Arctic **(c, d)**, and Barents Sea **(e, f)**. The individual models are presented in different colors. Time series have been smoothed with a five year running mean. The thick black lines represent the multi-model mean.

TCD
9, 1077–1131, 2015

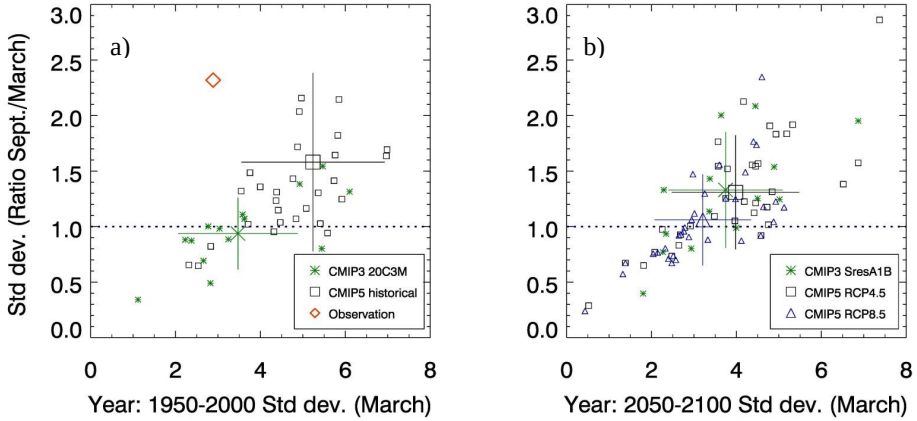

Figure 9. Change of March sea ice area SD in the Entire Arctic (in 10^5 km^2) and the ratio between September and March SDs in **(a)** 1950–2000 and **(b)** 2050–2100. Small symbols depict results for individual models; large symbols are for the ensemble means. The bars indicate intra-ensemble SD.

TCD
9, 1077–1131, 2015

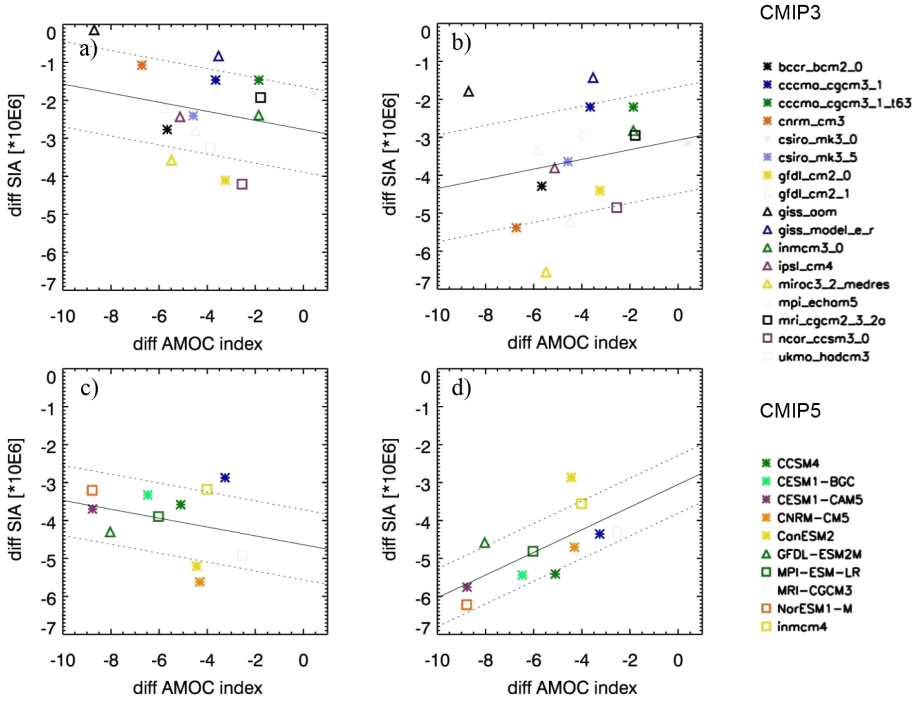

Figure 10. Changes (2070–2100 minus 1970–2000) of the Entire Arctic sea ice area (SIA) (km^2) in March **(a, c)** and September **(b, d)** as a function of the annual-mean AMOC index at 30° N as projected by CMIP3 (20C3M/SRES A1B; **a**, **b**) and CMIP5 (historical/RCP 8.5; **c**, **d**) models. The regression lines and RMS error of the regression are shown as solid and dashed lines, respectively.

TCD
9, 1077–1131, 2015

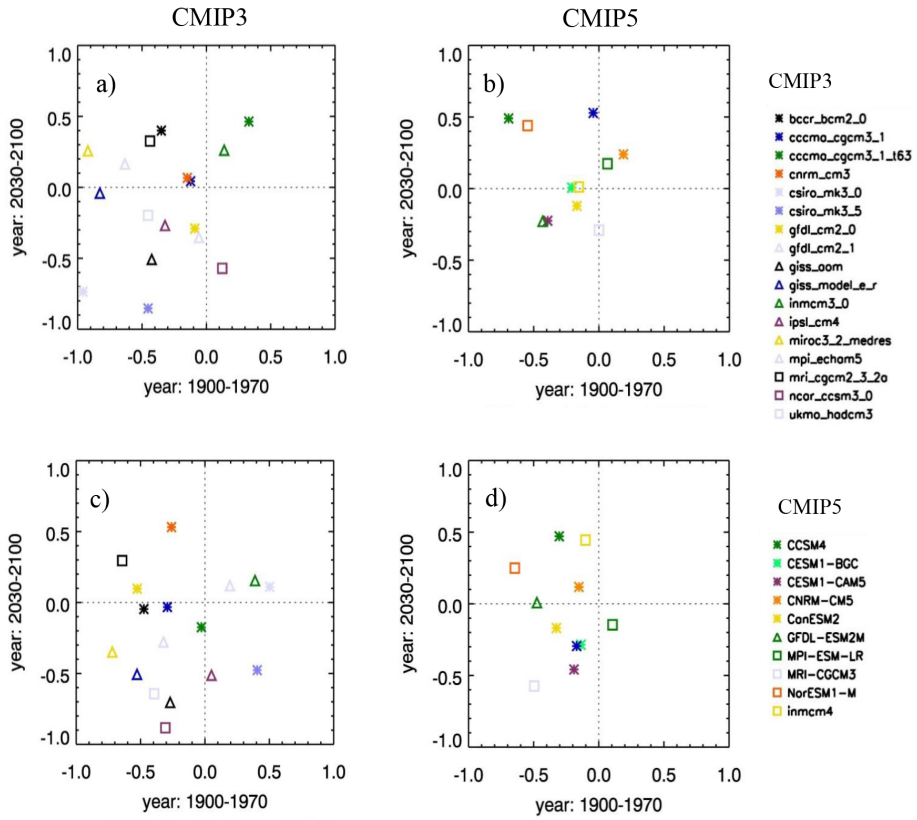

Figure 11. The correlations between the decadal variability of the AMOC index at 30° N and March sea ice area in the Entire Arctic **(a, b)** and Barents Sea **(c, d)** for CMIP3 **(a, c)** and CMIP5 **(b, c)** models during 1900–1970 and 2000–2070 periods. The strength of the correlation for 1900–1970 and 2030–2100 is shown on the *x* axis and *y* axis, respectively (see text for further details). The time series have been smoothed with 9 year running mean and detrended.

TCD
9, 1077–1131, 2015

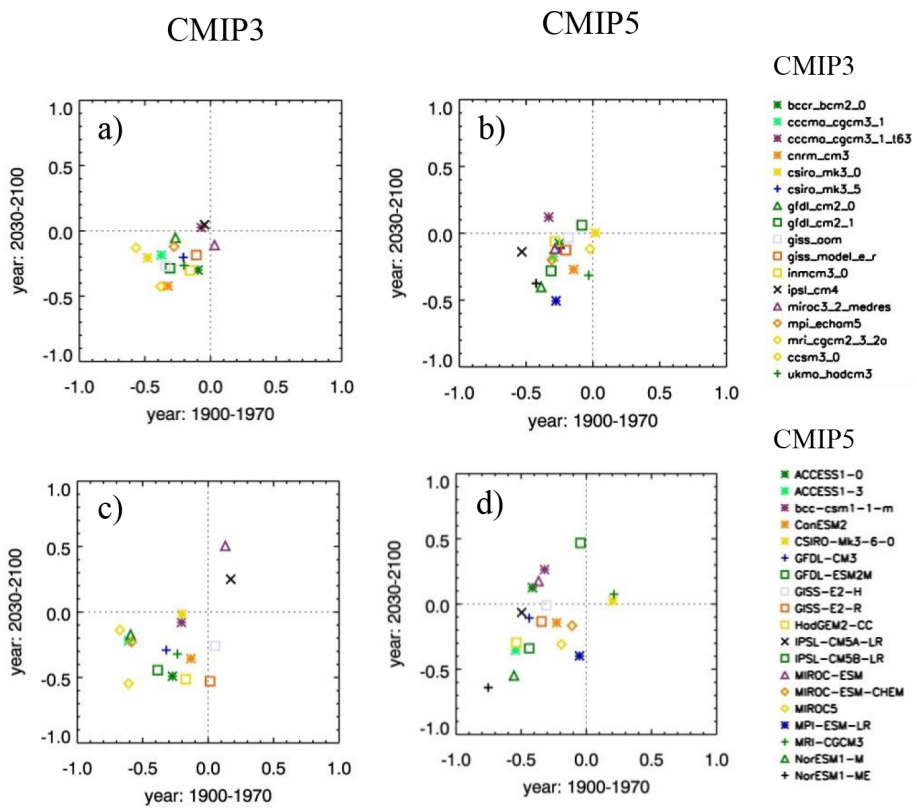

Figure 12. The correlations between the NAO index and March sea ice area in the Barents Sea as simulated by the CMIP3 **(a, c)** and CMIP5 **(b, d)** models during 1900–1970 and 2000–2070 periods. The strength of the correlation for 1900–1970 and 2030–2100 periods is shown on the *x* axis and *y* axis, respectively. Correlations have been computed using annual data **(a, b)** and after applying a 5 year running mean filter **(c, d)**.

TCD
9, 1077–1131, 2015

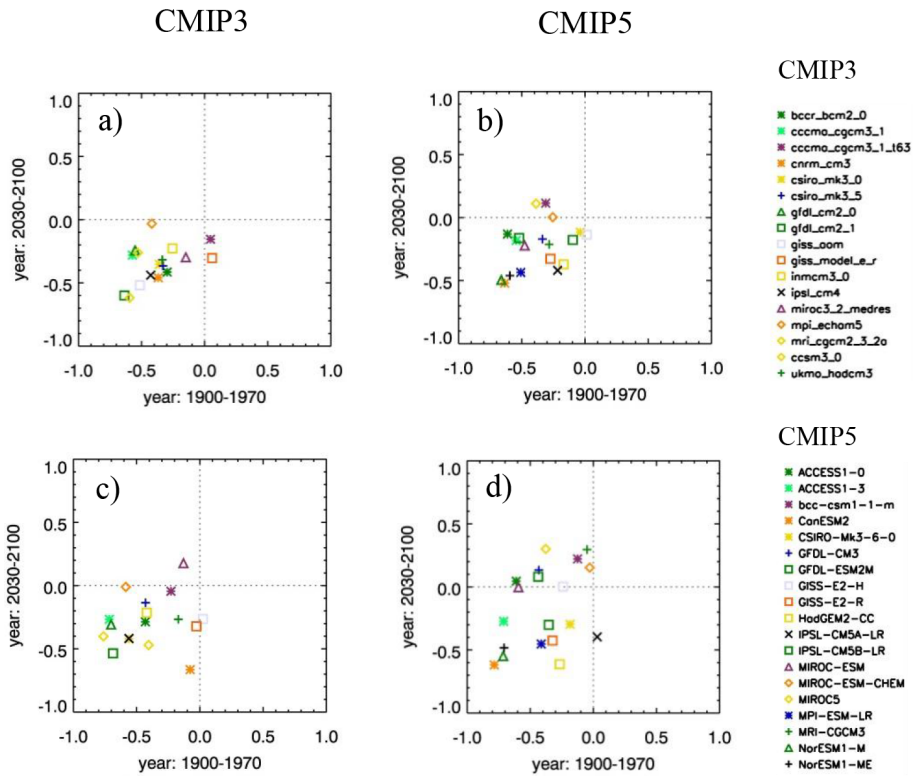

Figure 13. Same as in Fig. 12 but for the correlation of March Barents Sea sea ice area with the sea level pressure difference Scandinavia–Svalbard.

TCD
9, 1077–1131, 2015